
Article:
Hussain, Muhammad, Dhimish, Mahmoud, Titarenko, Sofya et al. (1 more author) (2020) Artificial neural network based photovoltaic fault detection algorithm integrating two bi-directional input parameters. Renewable Energy. pp. 1272-1292. ISSN 0960-1481

https://doi.org/10.1016/j.renene.2020.04.023

Artificial Neural Network based photovoltaic fault detection algorithm integrating two bi-directional input parameters

Muhammed Hussain, Mahmoud Dhimish, Sofya Titarenko, Peter Mather

University of Huddersfield, Laboratory of Photovoltaics, Huddersfield, HD1 3DH, United Kingdom

Abstract— In this paper, a fault detection algorithm for photovoltaic systems based on artificial neural networks (ANN) is proposed. Numerous literatures can be found on the topic of PV fault detection through the implementation of artificial intelligence. The novel part of this research is the successful development, deployment and validation of a fault detection PV system using radial basis function (RBF), requiring only two parameters as the input to the ANN (solar irradiance and output power). The results obtained through the testing of the developed ANN on a PV installation of 2.2 kW capacity, provided an accuracy of 97.9%. To endorse the accuracy of the newly developed algorithm, the ANN was tested on another PV system, installed at a remote location. The total capacity of the new system was significantly higher, 4.16 kW. A vital part of the test was to see how the proposed ANN would perform with 'scaled-up' input data, during normal operation as well as partial shading scenarios. The validation process provided an overall fault detection accuracy of above 97%. The decrease in accuracy was due to the varying nature of the two systems in terms of total capacity, number of samples and type of faults.

Keywords—Photovoltaics; Fault Detection; Artificial Intelligence; RBF Network.

1. Introduction

1.1 Research Background

Technological advancements in both hardware and software have enhanced the monitoring and analysis of grid-connected photovoltaic (GCPV) systems, for optimal energy harvesting along with reliable power production. The increase in the installation of PV due to its numerous benefits, means researchers are actively looking into the development of diagnostic methods for fault detection in PV plants.

PV systems process monitoring is based on a distributed sensor network (DSN), for analysis of the system and performance reviews. Corresponding time series analysis of obtained data is vital for statistical analysis of PV systems. The implementation of fault detection in PV systems can become complex depending on the variety of data being logged. A DSN may consist of several variables such as current, voltage, irradiance and temperature [1-2]. Therefore, the complexity of the process may hinder enterprises from implementing fault detection in their systems.

Researchers have proposed numerous methods to ease the complexity of failure detection systems by decreasing the number of input variables required, along with more sophisticated statistical analysis [3-4]. This paper proposes the use of Artificial Neural Networks (ANN) for this purpose.

Various fault detection techniques for PV systems are widely available in the literature, with varying accuracy levels, detection speed and algorithm complexity. Prediction of faults in PV systems through the unitisation of metrological and satellite data is one of the techniques used [5-6]. Whilst other fault detection algorithms for PV systems do not require any climate data [7].

Fault detection in PV systems can be split into three categories visual, thermal and electrical [8]. Before looking deeper into the electrical category, it is important to mention another technique which is also applicable, known as Electro Luminescence Imaging (EL). This technique is based on the solar module being supplied with external excitation current through its metal contacts, acting as a light emitting diode. A sensitive Si-CCDs camera can then take an image of the emitted photons at a wavelength greater than 850nm.

The electrical category is further divided into sub-categories consisting off:

- Methods that do not require any climate data (solar irradiance, temperature). An example of this approach is the Time-Domain Reflectometry (TDR) proposed in [9] for detection of disconnection of a PV string.
- Methods based around the analysis of the current and voltage characteristics. S. Silvestre *et al.* [10] calculates Series Resistance (R_s), Fill Factor (FF) and Shunt Resistance (R_{sh}) based on the I-V characteristics leading on to performance indicators. Fault detection for PV systems based on the evaluation of current and voltage indicators.
- Methods based around Maximum Power Point Tracking (MPPT). X. Li *et al.* [11] Proposes an automatic supervision and fault detection method based on power loss analysis. The approach led to the identification of faults including faulty module, faulty string and faults linked to partial shading, MPPT failure and ageing.
- Methods based on Artificial Intelligence (AI) techniques. Authors' in [12] look at the effectiveness of BP neural network for fault diagnosis in PV systems, comparing it to Fuzzy Logic. The author concludes BP neural network as the solution to most limitation faced through the implementation of Fuzzy Logic in fault detection of PV systems.

Artificial neural networks (ANNs) are mathematical tools, imitating biological human neural networks, learning from experience and generalizing previous behaviour as characteristics [13]. The ANN architecture consists of an input layer, one or more hidden layers and an output layer. ANN's ability to process information in non-linear, high-parallelism, fault and noise environments makes it of considerable interests to researchers in many fields [14-16]. In comparison to traditional model-based methods, ANN's are data-driven, self-adaptive methods learning from examples whilst picking-up subtle and hidden functional relationships that are otherwise unknown or hard to describe. In addition, ANNs are suitable for solving problems where explicit knowledge is difficult to identify, but a vast amount of data is available [17-19]. A. Lapedes *et al*. [20],

71 demonstrates how backpropagation neural networks surpass by order of magnitude any of the
72 conventional linear and polynomial methods dealing with chaotic time series of data. In addition,
73 A. Millit *et al*. [21] demonstrates ANN networks as a solution for the modelling and estimating of
74 output power for PV systems. Whereas, F. Polo *et al.* [22] proposes a failure mode prediction and
75 energy harvesting of PV systems to support dynamic maintenance tasks using ANN-based models.
76 Ultimately, it looks to analyse data and disregard the erroneous prediction of faults in a PV system.
77 The paper implements a back-propagation network, trained on historical data consisting of past
78 five years of an inverter used in the PV system. Highlighting the nature of failures under
79 consideration, the paper describes the faults as a result of equipment deterioration and useful life
80 reduction owing to operational and geographical features. The author in his conclusion claims that
81 the proposed methodology could further improve its performance if 'enough data' is available for
82 significant training of the ANN.

83 Yasuhiro Yagi *et al.* [23] proposes a learning method based on expert systems for the identification
84 of two types of faults (shading effect and inverters failure). The main advantage of this technique
85 is that it relies on simple and reprogrammable ANN network, but, on the other hand, the proposed
86 technique cannot identify faulty conditions occurring in PV systems such as PV short circuit failure
87 conditions and PV String failure. An advanced ANN network proposed by [24] demonstrates the
88 detection of faults in the DC part of a PV system such as faulty bypass diodes, faulty PV modules,
89 and faulty PV string. The paper proposes two algorithms based on MLP and RBF networks. The
90 confusion matrix shows the accuracy of the MLP (90.3%) was higher than that of RBF (68.4%).
91 It is a well-known fact that MLP networks, have a much higher accuracy as compared to RBF and
92 are more commonly used. Especially in networks requiring more hidden layers. However, it is also
93 important to note that MLP networks are more demanding in terms of computational time.
94 Therefore, if the use of multiple hidden layers is not required, then an RBF network can be
95 implemented saving computational time and appealing to a broader audience. However, the data
96 set consists of a modest number of samples (775). Also, the data set does not consist of real-time
97 data from a PV-system, but rather it is simulated using MATLAB/Simulink. Conversely, the data
98 sample used in our proposal consists of 97200 samples over a 10-week, obtained from a live
99 installation, refer to section 2.

100 Yuchuan Wu *et al.* [25] looks at the limitations of Fuzzy Logic used in early stages of fault
101 detection in PV systems. It highlights barriers such as the process for obtaining fuzzy rules and
102 membership function, along with the constancy of fuzzy systems. This method is implemented
103 using BP neural networks for fault detection in PV systems, resolving the issues faced with Fuzzy
104 logic through its ability to better self-learning, self-adaptability and non-linearity pattern
105 recognition.

106 1.2 Contribution and Paper Organization

107 The main contribution of this work is to present a novel algorithm that can carry out fault detection
108 in a PV system, to a high degree of accuracy, requiring only two inputs. This is done through the

implementation of an RBF network for the classification of the faults presented in section 3.2. The rationale for the selection of RBF over Multilayer Perceptron Networks (MLP) was due to the network only requiring a single hidden layer but more importantly due to RBF's robustness to adversarial samples in the data set. As proven in section 3.1, the ANN architecture accuracy was compared with a varying number of hidden layers. The results showed that a single hidden layer was the most optimal solution providing an accuracy of almost 99% while consuming the least amount of computational time. As a result of this an RBF network was selected rather than an MLP. Although MLP can also be used in a single hidden layer configuration, it demands more computational power, further discussed in section 3.8.

Rest of the article is organized as follows; Section 2 presents the examined PV installations. In section 3 we discuss in detail the rationale for selecting RBF over MLP and look at the structure of the proposed network along with the four different ANN-based methodologies to detect faults in PV systems. Section 4, looks at the results of the network. In section 5, we compare our developed ANN network with recent ANN-based models available in present literature. Finally, sections 6 and 7 present the conclusion and reference list, respectively.

2. Examined PV system

The overall system design is shown in Figure 1. The PV plant consists of 10 PV modules set-up in string topology, irradiance sensor, MPPT unit and DC- load. The input/output pins of the MPPT unit are linked via Ethernet-capable to a personal computer (PC) to facilitate real-time data monitoring. The proposed ANN algorithm for fault detection of the PV modules is developed in MATLAB software.

As shown in Figure 2, the PV plant consisting of 10-polycrystalline silicon PV modules, with a nominal power of 220 W (per module), the electrical parameters under 'standard test conditions' (STC) of the PV modules are shown in Table 1; STC of the PV modules at solar irradiance = 1000 W/m^2, module temperature = 25 °C, spectral distribution of the incident light according to AM 1.5 and irradiation perpendicular onto the receiving plane. The Maximum Power Point Tracker (MPPT) has an output efficiency of not less than 95.0%. Internal sensors within the MPPT are used to measure the DC current and voltage.

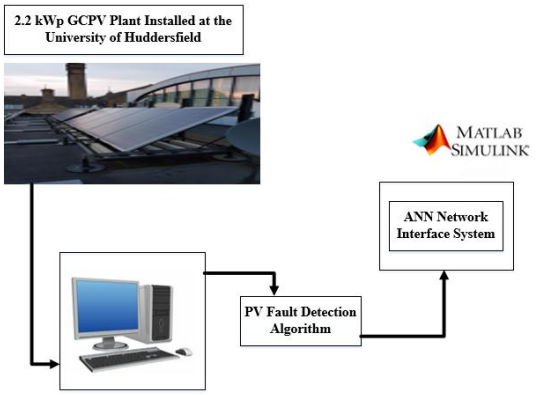

Figure 1. Overall System Architecture Design for the Examined PV Plant

Table 1. Electrical characteristics of SMT6 (60) P PV module

Solar Panel Electrical Characteristics	Value
Peak Power	220 W
Voltage at maximum power point (V_{mpp})	28.7 V
Current at maximum power point (I_{mpp})	7.67 A
Open Circuit Voltage (V_{oc})	36.74 V
Short Circuit Current (I_{sc})	8.24 A
Number of cells connected in series	60
Number of cells connected in parallel	1
Series resistance R_S	0.53 Ω
Parallel resistance R_{sh}	1890 Ω

Davis weather station measures the global solar irradiance, which is passed onto the monitoring unit connected to the PC for data recording and monitoring. A Hub 4 communication manager facilitates acquisition of modules temperature via the Davis external temperature sensor, as well as the electrical data for each photovoltaic string.

The weather station is located on the same level and position of the PV modules, as presented in Figure 2(a). The weather station is mounted near to the examined PV system, the solar irradiance is measured using a pyranometer which has a resolution of ±2 W/m^2, while the angle of incident is set the same as the PV modules inclination of 37 degrees.

If the angle of inclination is changed, therefore, the results of the solar irradiance would typically impact the ANN detection accuracy, since the solar irradiance against the output predicted power would be expected to be inaccurate. For generalization purposes, it would be more appropriate to use a mathematical modeling for the solar irradiance which can predict the output irradiance on a particular location including the inclination of a typical PV system, this was not the case in our model, as we ensure that the pyranometer is on the same inclination as the examined PV installations.

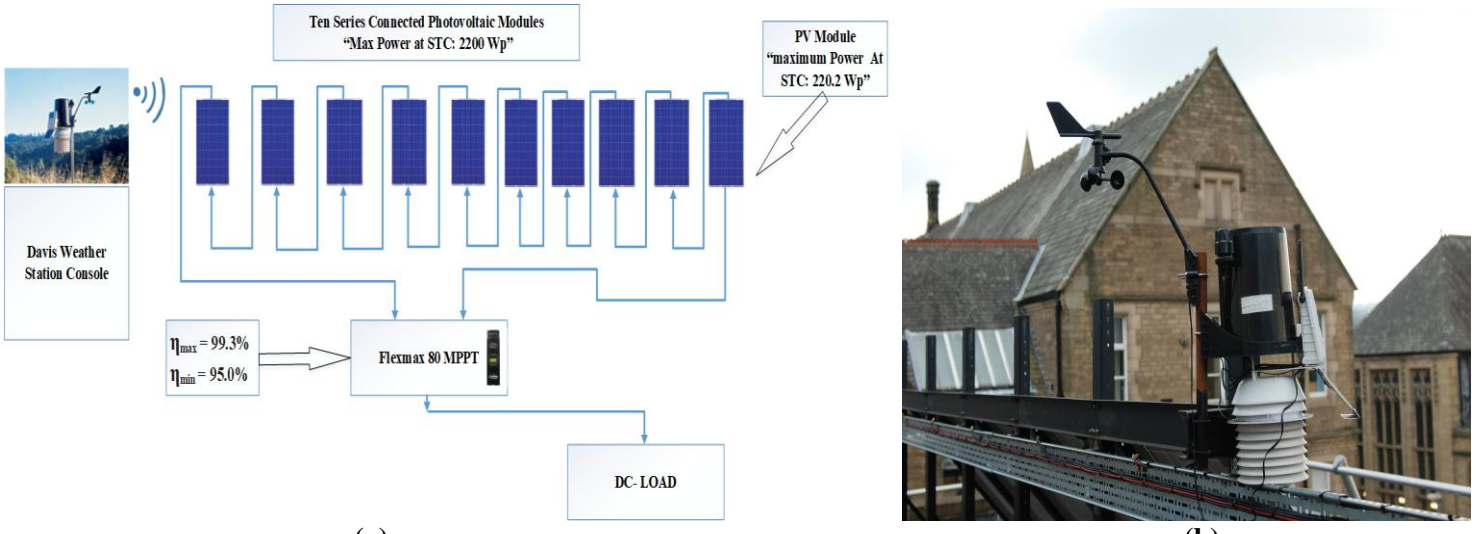

Figure 2. **(a)** Examined PV System layout including the weather station and DC-Load, **(b)** weather station mounted in the examined PV installation

In this article, we have taken a data samples of the PV installation captured over a commencing period of November 2019 to February 2020. As a result, it might be useful to outline that during summer period, when the irradiance and ambient temperature is expected to have a high peak, the prediction and accuracy of any typical ANN network might differ. Hence, in the following section, we have used four different data input setups to overcome this issue.

3. Methodology

Researchers have demonstrated various methodologies for data normalisation, training, validation and testing of ANN networks. To the best of our understanding, the majority of the implemented methodologies found in recent literature are based on data sets, consisting of several inputs to the network [5, 21 & 24]. The following sub-sections demonstrate in detail the four methodologies that were implemented on the sample data set consisting of solar irradiance and total output power. The data consisted of 10 weeks, one week worth of data for every fault, starting with normal operation (NO). The ANN was trained with each methodology and the overall detection accuracy for the four methodologies is used as a reference to the success of each.

3.1 ANN Structure

The purpose of the ANN was to detect faults in PV modules, as shown in Figure 3. Before the ANN could be trained with a sample data set, the first step was the formation of a strategy, to test the optimal process for selecting the sample data to train the ANN. For this critical task, four different methodologies for data processing were investigated:

1. Methodology 1 (M1): solar irradiance and output power was randomly selected, including all off-state data (where power is equal to zero), no normalisation process was involved.
2. Methodology 2 (M2): solar irradiance and output power was randomly selected, all off-state data was dismissed, no normalisation process was implemented.
3. Methodology 3 (M3): solar irradiance and output power was randomly selected and normalised using the max-min normalisation technique.
4. Methodology 4 (M4): solar irradiance and output power was randomly selected and normalised. In addition, solar irradiance of 0 - 1000 W/m^2 was mapped along with the output power.

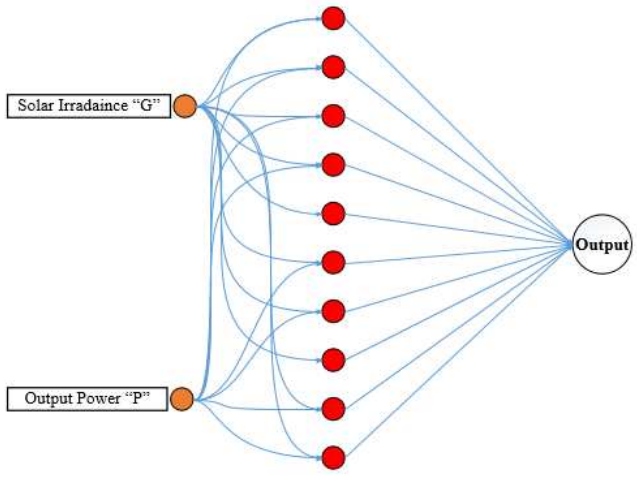

Figure 3. The proposed RBF architecture

The architecture of the ANN was based on the Radial Basis Function (RBF). The network was made up of three parts (input, hidden layer and output). For this research, a single hidden layer was implemented, for all investigative methods, due to the linear nature of the response, high accuracy and minimal computational time. The hidden layer can be increased for further accuracy and computational performance, depending on the application under consideration. Increasing the number of hidden layers would convert the network into an MLP, increasing the computational time. The developed ANN architecture using one hidden layer achieved a high rate of detection accuracy, almost equal to 99%; this will be discussed in the following sections.

In principle, each neuron takes a formed linear combination of the outputs of previous neurons. This linear combination is weighted through the strength between the neurons (w_{ij}) and multiplied by the input (x_j). Further, the activation threshold (w_{j0}) is also assigned to each neuron. This process is expressed using (1). Note: i is equal to number of hidden neurons (1, 2, 3 … 10), j is equal to number of inputs (1 and 2).

$$\sum_{j=1}^{n}(w_{ij}x_j + w_{j0}) \tag{1}$$

Next, the weighted activation process is then multiplied by the non-liner function f_1 as shown in (2), this is usually a sigmoid function (MLP) or Euclidian function (RBF). Finally, the output value of the hidden layers y_i is expressed by (3).

$$f_1 \times \sum_{j=1}^{n}(w_{ij}x_j + w_{j0}) \tag{2}$$

$$y_i = f(u) = \frac{1}{1+ e^{-\sum_{j=1}^{n}(w_{ij}x_j + w_{j0})}} \tag{3}$$

in order to enhance the performance of the selected ANN structure, we have used the quick prorogation method, expressed by (4), where the tanning iteration number is equal to 1000.

$$\Delta w(s) = \frac{\nabla\delta|w(s)}{\nabla\delta|w(s-1) - \nabla\delta|w(s)} \Delta w(s-1) \tag{4}$$

where δ is the error function of the simulation process, w is the vector of the weights for the developed ANN network shown in Figure 3, and s is the iteration number. The best layout of the developed ANN network is also shown in Figure 4.

The developed structure of the ANN network is shown in Figure 4(a). The RBF network with two inputs, one hidden layer and 10 hidden neurons is selected. In fact, the selection of the inputs was obtained using the available parameters from dataset, including the solar irradiance (G) and the output power (P). The selection of the hidden layers is obtained using an extensive simulation from 1 to 100 hidden layers; as a result, ten hidden layers were selected due to its optimum performance. The results of the ANN network accuracy vs the number of hidden neurons used for the considered methodologies (M1, M2, M3, and M4) is shown in Figure 4(b). It is noticed that the last adopted methodology achieved the highest ANN detection accuracy of 98.6% using 10 hidden neurons. The minimum ANN accuracy of 40.2% is observed for the first methodology using 90-100 hidden neurons.

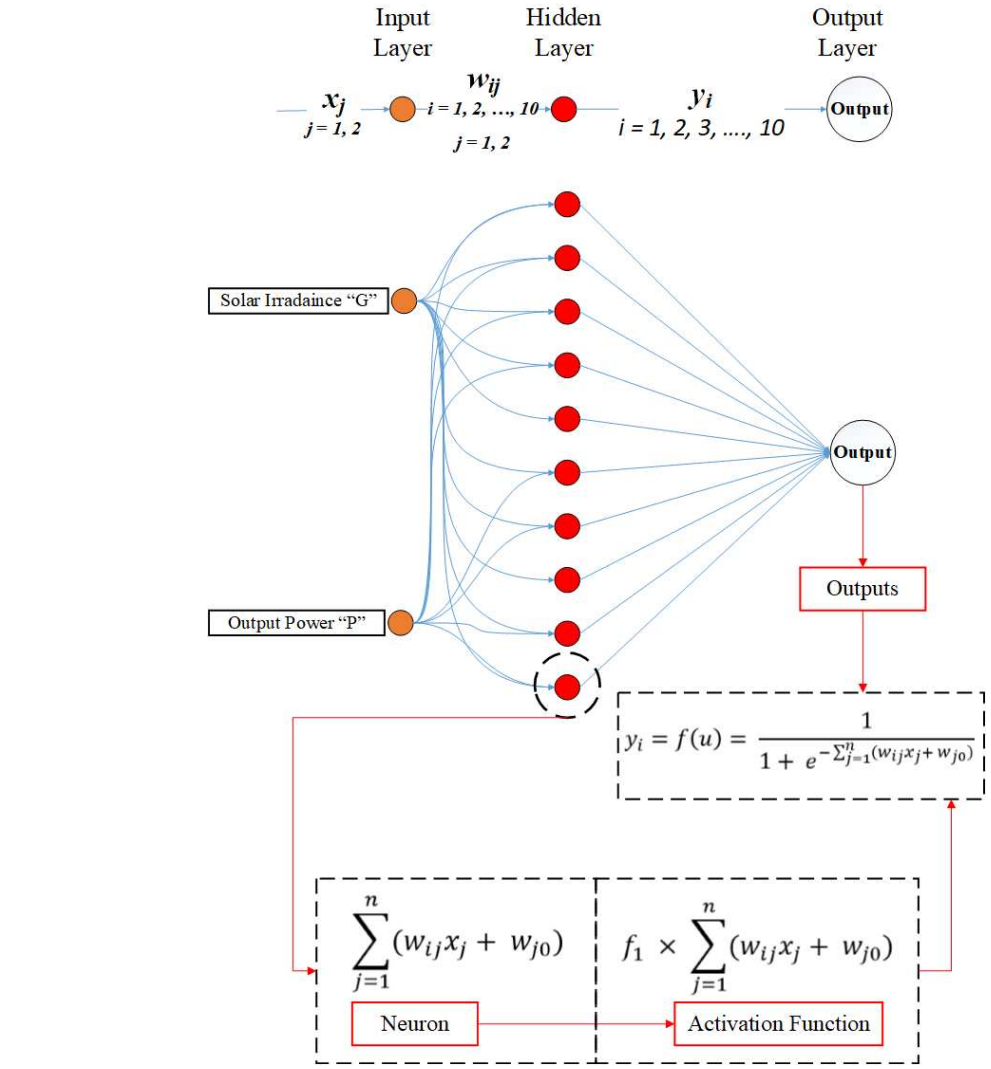

(a)

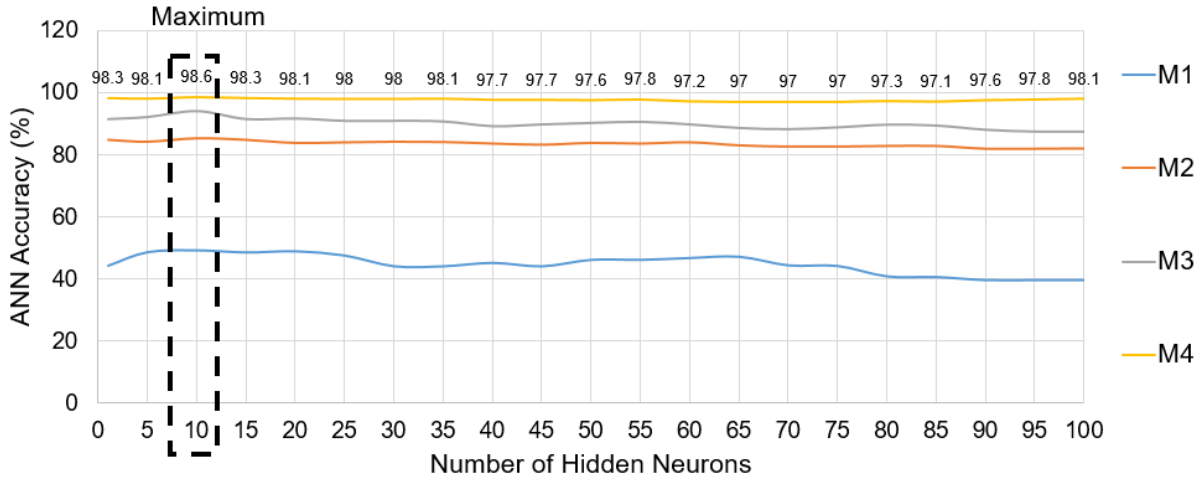

(b)

Figure 4. **(a)** Details of the proposed ANN network architecture, **(b)** ANN accuracy vs number of hidden neurons

3.2 ANN Network Training and Validation

Before the training and validation process began, the faulty conditions considered for the ANN to detect had to be identified. In this article, 10 different scenarios have been taken into consideration, presented as follows:

- Case1: Normal operation mode, where no faults were applied to the PV string
- Case 2: 1 Fault applied to the system; 1 PV module disconnected from the PV string
- Case 3: 2 Faults applied to the system; 2 PV modules disconnected from the PV string
- Case 4: 3 Faults applied to the system; 3 PV modules disconnected from the PV string
- Case 5: 4 Faults applied to the system; 4 PV modules disconnected from the PV string
- Case 6: 5 Faults applied to the system; 5 PV modules disconnected from the PV string
- Case 7: 6 Faults applied to the system; 6 PV modules disconnected from the PV string
- Case 8: 7 Faults applied to the system; 7 PV modules disconnected from the PV string
- Case 9: 8 Faults applied to the system; 8 PV modules disconnected from the PV string
- Case 10: 9 Faults applied to the system; 9 PV modules disconnected from the PV string

It is worth noting that the partial shading considered in this research is when a PV module is affected by either shading caused by moving clouds or when an overcasting weather condition is arisen. Hence, no applied shading was practiced as we tried the best to comply with real shading scenarios rather than using opaque objects like some research do. For that reason, we took long-term data measurements of the PV installation over a period of 10 weeks, rather than simply reliant on simulated or applied shading conditions which can be operated over couple hours.

Figure 5 shows a flowchart of the proposed fault detection architecture. Initially, the measured output power of the PV string was attained using the MPPT unit. If the output power was greater than zero, the measured power was passed into the developed ANN network. In case the output was equal to zero, verification of the measured voltage had to be carried out to decide whether the PV string was faulty (voltage > 0), or in sleep mode (V = 0).

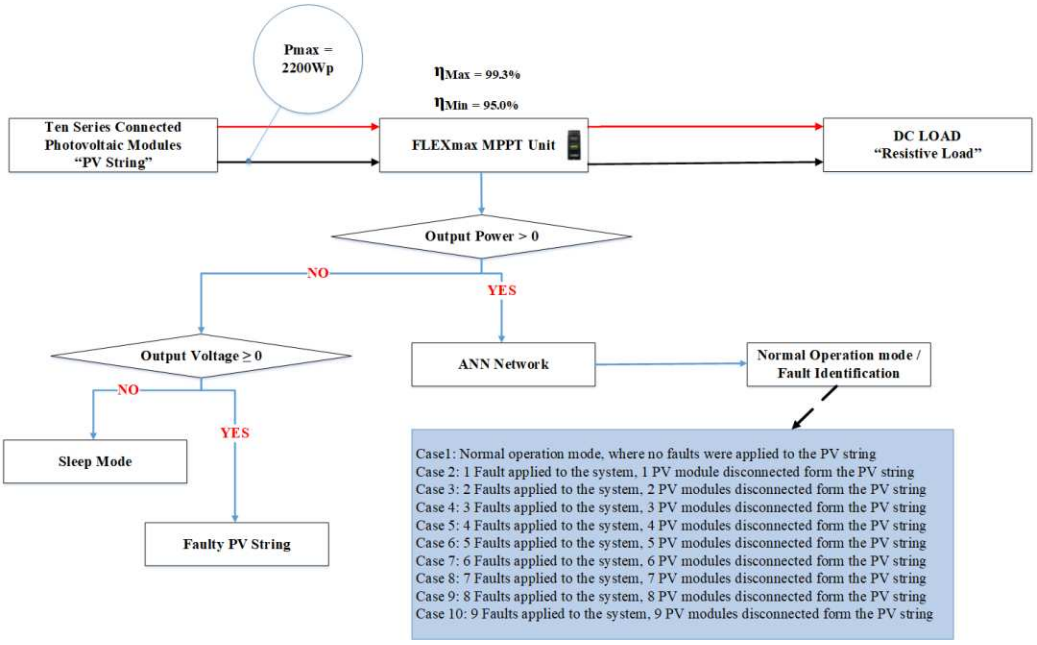

Figure 5. Flowchart of the proposed fault detection algorithm

In order to practically testify the examined faulty scenarios, we have used the junction-box placed next to the PV installation in which we can apply any faulty condition to the PV string, and this junction-box can be configured manually using a switch-connection where a PV module(s) can be connected or disconnected from the PV string.

For instance, Figure 6 shows three case scenarios applied to the PV installation including case 1 "normal operational mode", case 2 "one PV module is disconnected from the PV string", and case 5 "four PV modules are disconnected from the PV string".

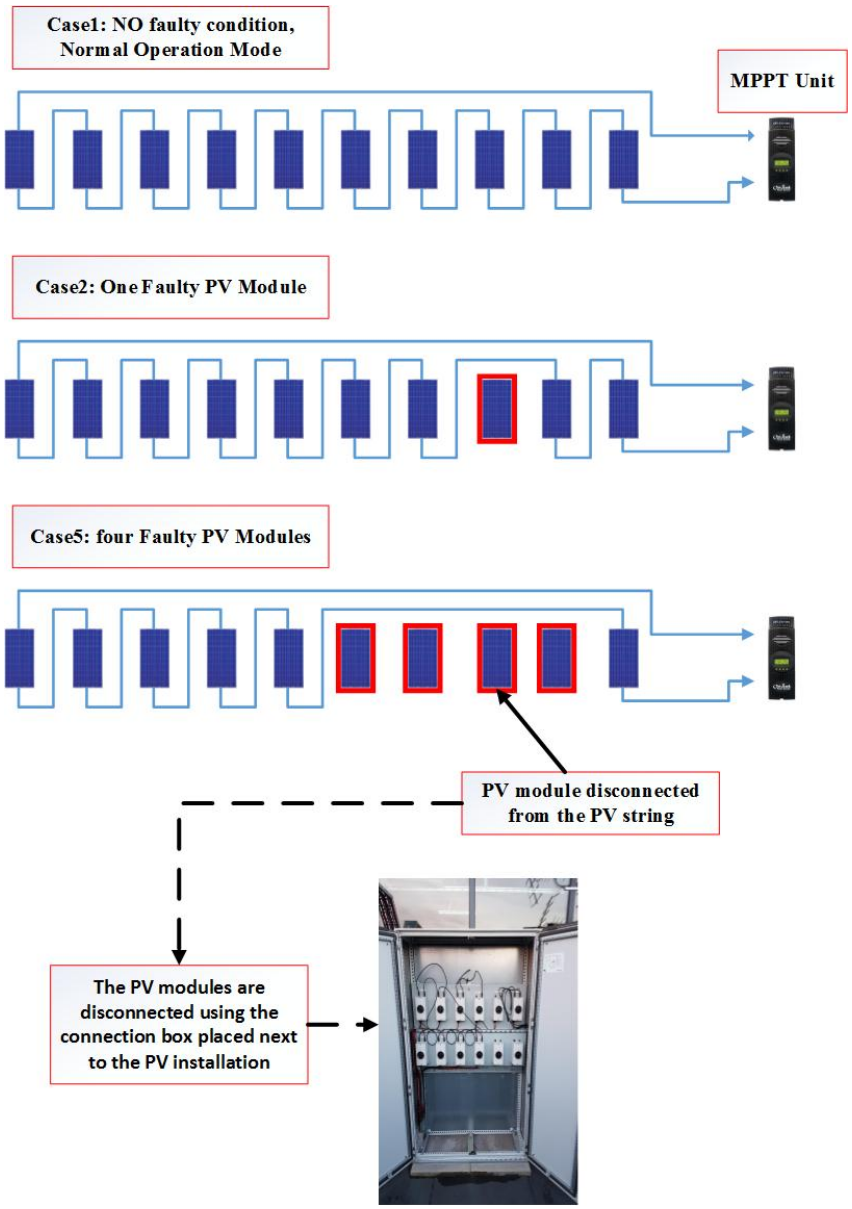

Figure 6. Schematic shows two applied cases on the examined PV installation

The data set used for training the ANN was recorded from the experimental PV setup shown previously in Figure 2. During the experiments, the value of solar irradiance and total power were logged, with the PV modules' temperature between 9.8 – 24.6 ^{0}C. As the proposed ANN model does not require the temperature of the solar modules; hence, this value was not taken into consideration. The data set shown in Figure 7 of the solar irradiance and the output power, consists of 97200 measurements captured for 10 weeks. Each week corresponds to a different condition.

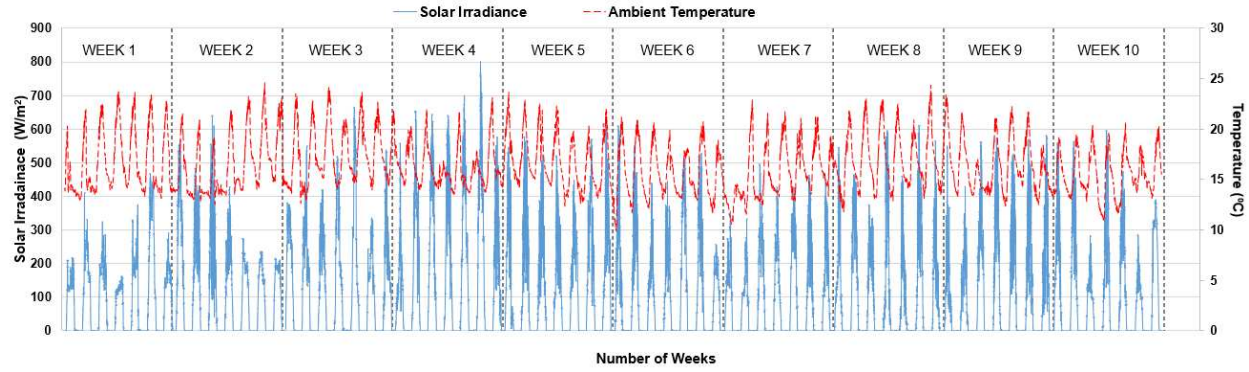

(a)

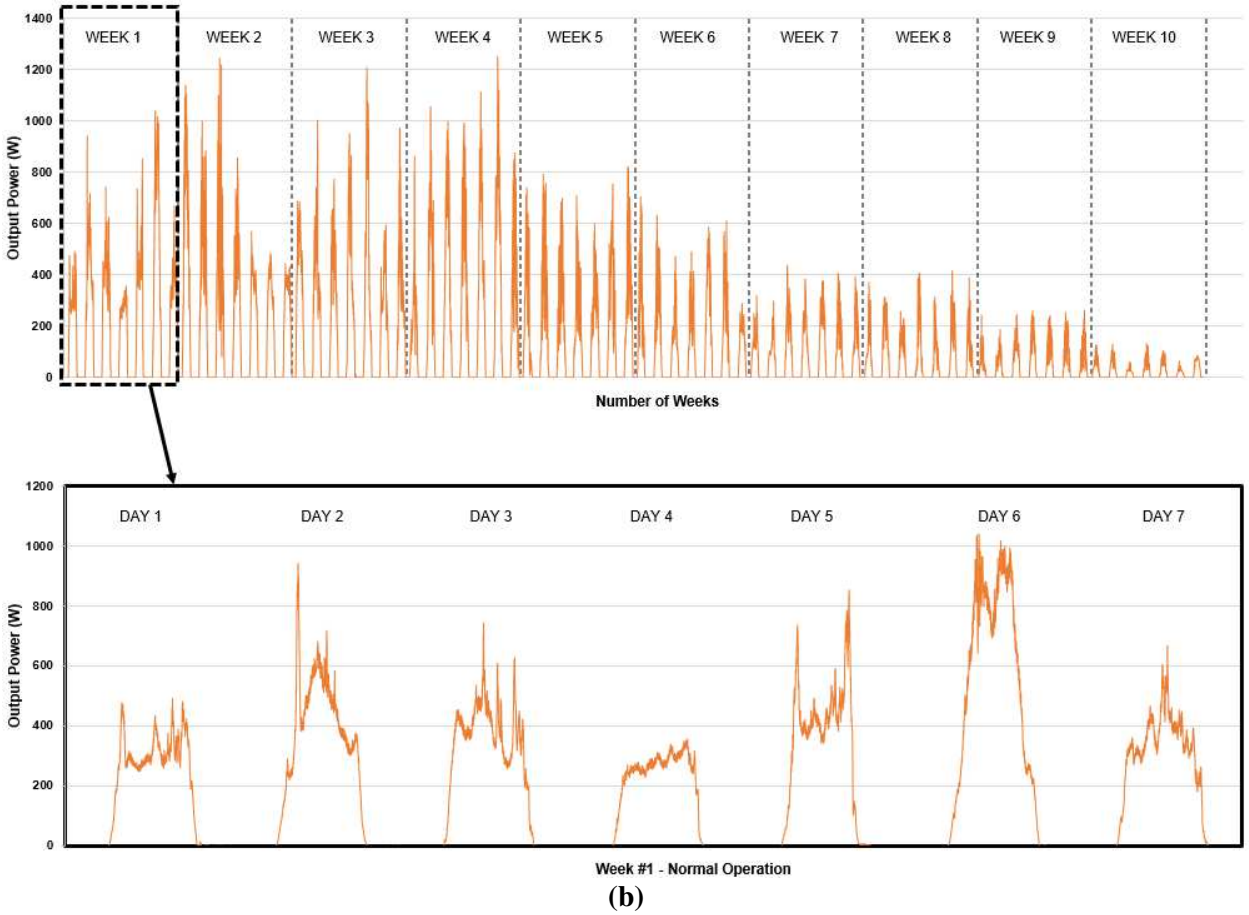

(b)

Figure 7. Data set used for training purposes; 97200 samples, each scenario has 9720 samples gathered over ten weeks. **(a)** Solar irradiance, **(b)** Output PV power

Various methodologies available in literature [5, 21, 24, and 26] used training samples for one to three days for faulty conditions. While in our case, the data was recorded over a duration of one week for every faulty condition. Another limitation of the recent work, 2019, conducted by [27 and 28] is that the ANN networks were trained using various inputs such as PV string voltage, current, solar irradiance, power and ambient temperature. Whereas our proposed ANN network only requires solar irradiance and output power as an input for the network. Note, a brief comparison of the accuracy will be discussed later in section 5.

It is worth noting as the number of faults increases on a week-by-week basis, the total output power measured for the PV system deteriorated, as shown in Figure 8.

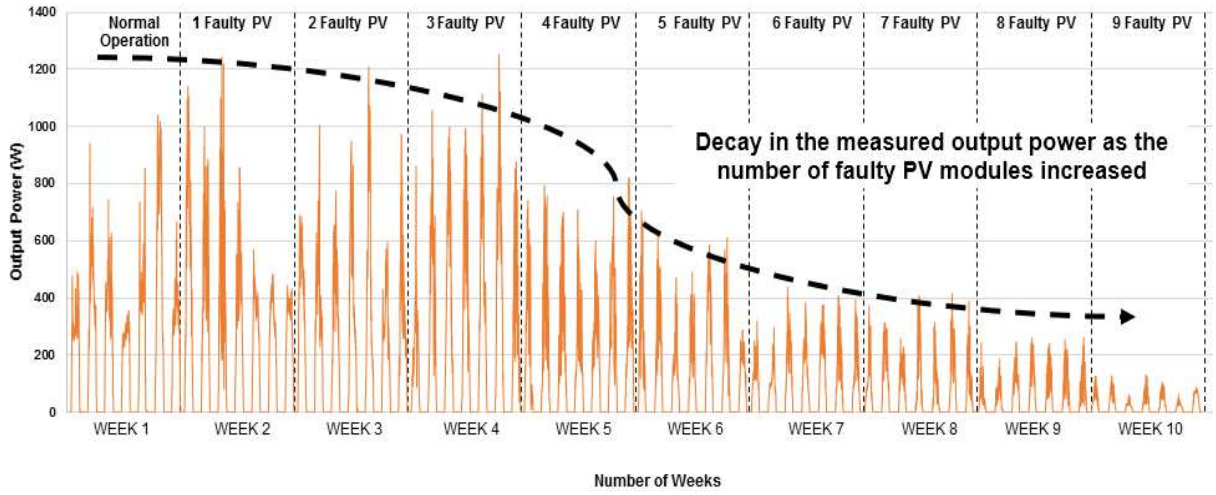

Figure 8. Flowchart of the proposed fault detection algorithm

As part of some methodologies (M3 and M4) which will be discussed in the following sub-sections, the normalisation process of the input data for the solar irradiance and output power had to be carried out.

The standard input parameters used to configure all tested ANN models are the solar irradiance (G) and total output power (P). The Data set (input variables) are normalised using the max-min normalisation technique, within the range of 0 and +1 using (5).

$$y = \frac{(y_{max} - y_{min})(x - x_{min})}{(x_{max} - x_{min})} + y_{min} \quad (5)$$

where $x \in \{xmin, xmax\}$ is the original data value, and $y \in \{ymin, ymax\}$ is the corresponding normalised value with $ymin = 0$ and $ymax = +1$."

3.3 Implementation and Validation of the First Methodology (M1)

The ANN network was trained with randomly selected solar irradiance and output power, including non-representative data (represented by a zero for power), no normalisation of sample data was carried out in this approach. The ANN achieved an overall detection accuracy of 49.4%, refer to Figure 9(a). Many factors could have contributed to the low accuracy of the network. One possible factor was the inclusion of 'non-representative' data denoted by a zero, either for solar irradiance or PV output power.

3.4 Implementation and Validation of the Second Methodology (M2)

This methodology looks to improve the accuracy of the ANN by addressing the possible cause highlighted in M1. The input parameters (solar irradiance and output power) were randomly selected, but all 'non-representative' data was removed from the sample set which was to be used for training the network. The ANN network achieved an improved overall accuracy of 85.4%, refer to Figure 9(b). However, this is still considered as low accuracy for an ANN. This could have been due to no normalisation of data being carried out on the selected sample set.

For ANN networks training and validation, every dataset does not require normalisation. It is required only when features have different ranges. In our case, normalisation process would be expected to enhance the accuracy of the ANN as both ANN inputs, solar irradiance and output power, have a divergent range, i.e. the solar irradiance ranges from 0-1000 W/m^2, while the output power ranges from 0 to 2200 W.

The green and red cells of the matrix represent the number of correct and incorrect classifications by the ANN, respectively. The grey cells represent the total detection accuracy with respect to each row and column. The number 1, represents 1- fault (F1) and so on, ending at 10- faults (F10).

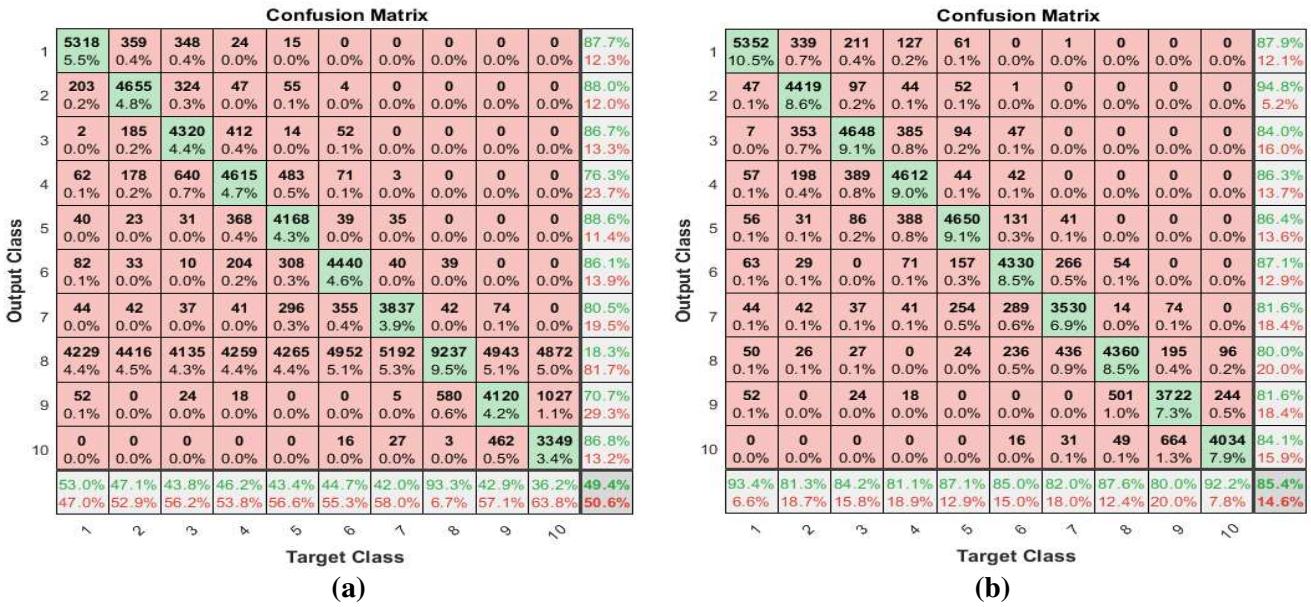

Figure 9. Output confusion matrix. **(a)** M1, **(b)** M2

3.5 Implementation and Validation of the Third Methodology (M3)

For the development of the third methodology, we have considered the previous methodologies (M1 and M2), but also included the normalisation of the sample set data before training the ANN network. The overall detection accuracy of the ANN using this approach was 94.2%, refer to Figure 10. An improvement can be seen as compared to the above approaches due to the normalisation of data before training the ANN. However, normalisation does not cater for missing data samples between two data points. For example, the normalised data of the solar irradiance may include values from 500 and 505 but not the values in between. This issue is further explored in the implementation of the fourth ANN architecture.

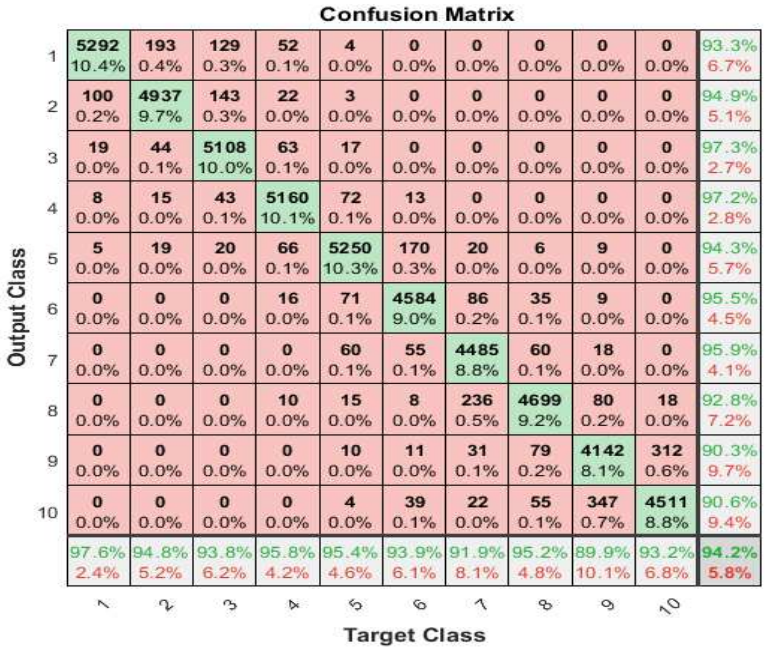

Figure 10. Output confusion matrix obtained using M3

3.6 Implementation and Validation of the Fourth Methodology (M4)

The normalised data of the solar irradiance or output power may include value, for example, 500 and 505 but not the values in between. This method implemented the concept of 'mapping' sample data set, before feeding it into the ANN for training, validating and testing purposes. Through the implementation of mapping input parameters, all values within the defined data points are taken into account. The ANN was trained using randomly selected data set, no "off-state" data was involved, normalisation process had been implemented, and finally the novel part of this approach, the mapping feature of the solar irradiance against the PV system output power was implemented.

The solar irradiance 0 - 1000 W/m^2 was mapped along with the corresponding output power as shown in Figure 11(a), with a step size of 1 W/m^2. The accuracy of the ANN improved significantly (98.6%) compared to the prior methods, as presented in Figure 11(b).

As suggested, the rationale behind the mapping of the inputs was to try and obtain a complete dataset before training the network. This was made possible due to only having two inputs. However, datasets containing multiple variables such as temperature, wind speed, voltage along with irradiance and power would make the task more difficult.

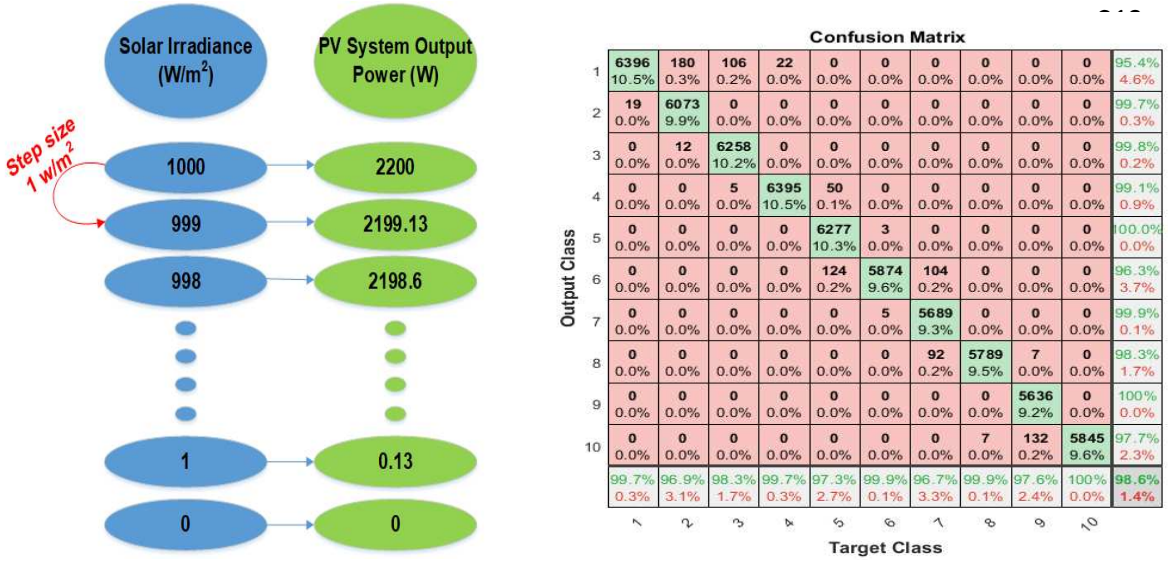

(a) **(b)**

Figure 11. **(a)** Mapping solar irradiance and PV system output power, **(b)** Confusion Matrix for M4

3.7 Evaluation of the Four Developed Methodologies

The overall detection accuracy of the ANN based on the four methodologies is presented in Table 2. A key observation to take away from Table 2, is the importance of data normalisation before proceeding with the training of the ANN. M1, had the least detection accuracy (49.4%). This was primarily because the raw data extracted from the PV setup shown in Figure 2, was directly used to train the ANN without filtering noisy data. The dismissal of 'off-state' data (M2), significantly improved the accuracy of the network (85.4%). Normalisation (M3), further improved the detection accuracy (92.2%) thanks to the sync of the input range, with (M4) achieving the highest detection accuracy due to the mapping of inputs to cater for missing data points.

Table 2. Evaluating all developed methodologies

Methodology No.	Training data set including solar irradiance and output power	Training Data does not include "off-state" samples	Normalisation Process of the training data set	Mapping 0-1000 W/m^2 into the actual output power	ANN network detection accuracy (%)
M1	✓	✗	✗	✗	49.4
M2	✓	✓	✗	✗	85.4
M3	✓	✓	✓	✗	92.2
M4	✓	✓	✓	✓	98.6

The critical element in increasing the ANN-network detection accuracy is principally due to the increase of the ANN receiver operating characteristics (ROC) during the training, validation and testing stages. The ROC is a graph showing the performance of a classification model at all classification scenarios (i.e. class 1 corresponds to case1 "normal operation mode", while class 10 corresponds to case 10 "9 faulty PV modules").

As can be noticed in Figure 12(a), during the training and validation of methodology 1, the ROC tends to have a high false-positive rate which at the end reduces the overall detection accuracy of the ANN network. Comparatively, Figure 12(d) shows the ROC for the last methodology, while it is evident that the true-false rate has significantly decreased, there is an increase in the true-positive rate due to the impact of the normalisation and the mapping procedure implemented during the data handling processing stage, resulting in the highest rate of detection accuracy of 98.6%.

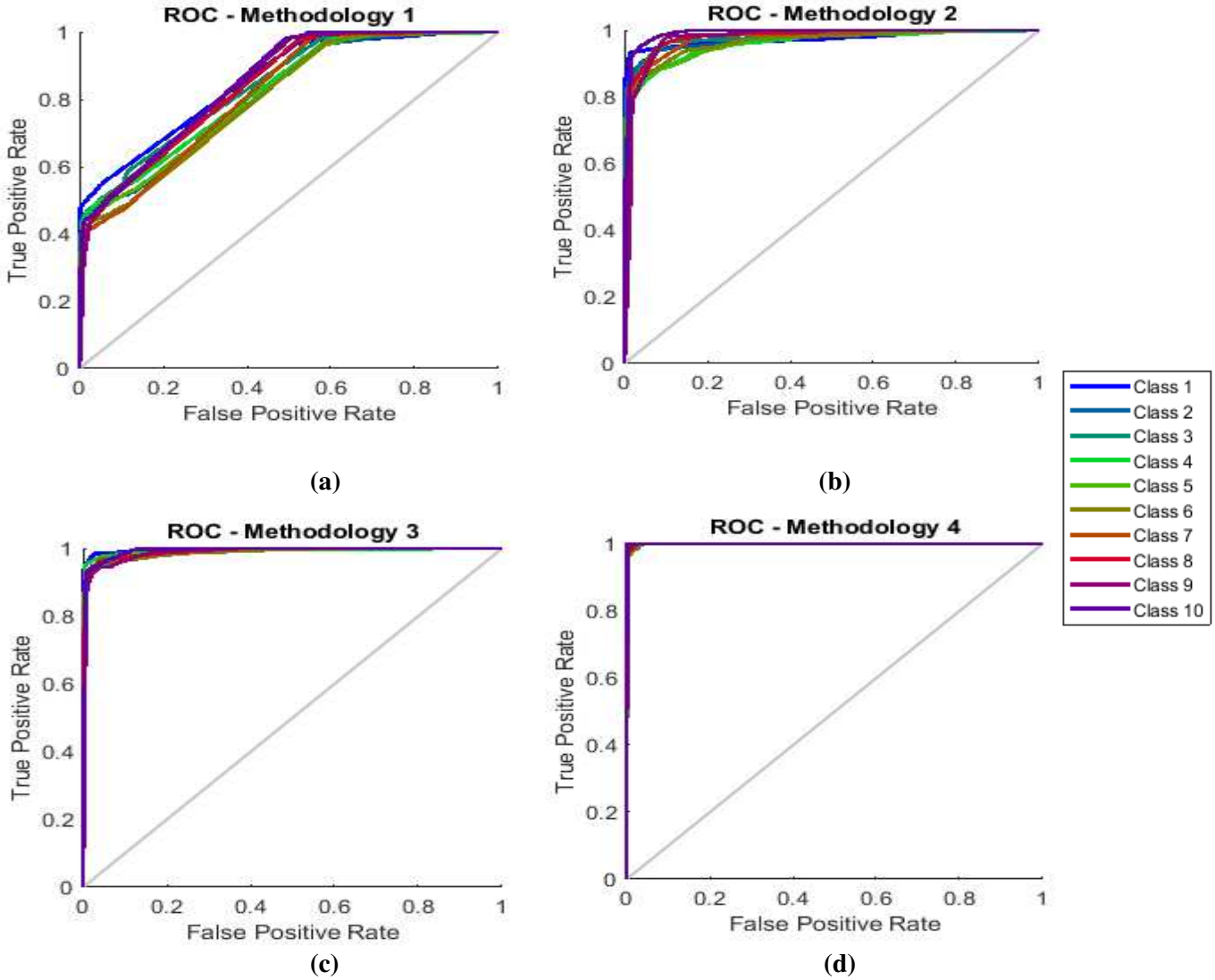

Figure 12. ROC performance of each ANN methodology. **(a)** M1, **(b)** M2, **(c)** M3, **(d)** M4

According to what has been discussed so far, it is worth noting that the rationale for the selection of RBF over Multilayer perceptron networks (MLP) was due to the network only requiring a single hidden layer but more importantly due to RBF's robustness to adversarial samples in the data set. As proven in this section, the ANN architecture accuracy was compared with a varying number of hidden layers. The results showed that a single hidden layer was the most optimal solution providing an accuracy of almost 99%. As a result of this an RBF network was selected rather than an MLP. Although MLP can also be used in a single hidden layer configuration, it demands more computational power.

The first novelty this research brings to the field of PV fault detection through ANN, is the use of only two inputs for training the network, i.e. solar irradiance and output power. While the authors acknowledge that the introduction of smart meters provide an effective platform for obtaining various inputs used for training ANN, without having major implications in terms of more hardware, there are other issues which are introduced as a result. The use of, for example, a five inputs ANN-based fault detection system rather than two means more time must be spent on data processing. It is, in fact, this stage of the process in the development of an ANN which directly impacts the overall accuracy of the network. If the network requires five inputs, the smart meter will be able to provide this data, but the problem occurs when the data must be processed for training the network as additional inputs result in more time required for data censoring and higher chances of non-representative data making its way into the network due to human error. Whereas, by limiting the inputs to only two, as proposed in this article, less time and effort is required for data processing, less chances of noisy data leaking into the training stage and ultimately a higher performing network, as evident from section 4.

In addition, as we have used solar irradiance data, academics, industry and national interest alike are demanding this data for various reasons such as predicting the ambient temperature, techno-economic analysis of the heating systems, transportation sector, etc. Therefore, we do not consider acquiring solar irradiance is a major drawback of this research, since, as an example, the UK Met-office[1] have a live grid climate variable system to download live solar irradiance as well as forecasted data; this approach of making live data for public use is now widely held in various counties such as Spain, Italy, and Singapore.

Another novel part of this research (principally using the fourth methodology) is the mapping of the inputs after removing non-representative data and carrying out data normalisation. A fundamental component within this methodology which plays a vital role in achieving high accuracy is the selection of the 'step size' for the mapping. A step size of 'one' was selected as shown in Figure 11. The rationale for not selecting a step size of '10' was due to under-fitting. As the gap between the data points would make it difficult for the network to be able to generalize. Conversely, a step size of less than one, for example '0.5', would force the network to accurately map the data points without generalizing, resulting in a network that is unable to accurately classify new input data, rendering it as an 'over-fit' network.

[1] https://www.metoffice.gov.uk/research/climate/maps-and-data/data/haduk-grid/haduk-grid

3.8 RBF vs. MLP

RBF and Multi-Layer Perceptron (MLP) are both neural networks as shown in Figure 13. Both networks have some common features but also significant differences in the way they operate, which makes one network more suited for certain applications as compared to the other. The well-known difference between the two networks is that RBF only uses a single hidden layer, whilst MLP can accommodate multiple hidden layers.

Both RBF and MLP networks can be used for regression and classification problems. Also, both networks have the capability to approximate complicated functions. However, RBF's have explicit local representations as each neuron represents a specific region of the input space. Conversely, in an MLP network, each neuron tries to capture a specific feature from the training set. Early neuron layers capture low-level features and as the information propagates through the hidden layers the feature extraction matures. This can optimize the overall accuracy of the network but at the expense of increased computational power, a trade-off which comes down to the objectives of the project. As there is only one hidden layer in an RBF network, each neuron captures the similarity between the whole training set and the center of the Euclidian.

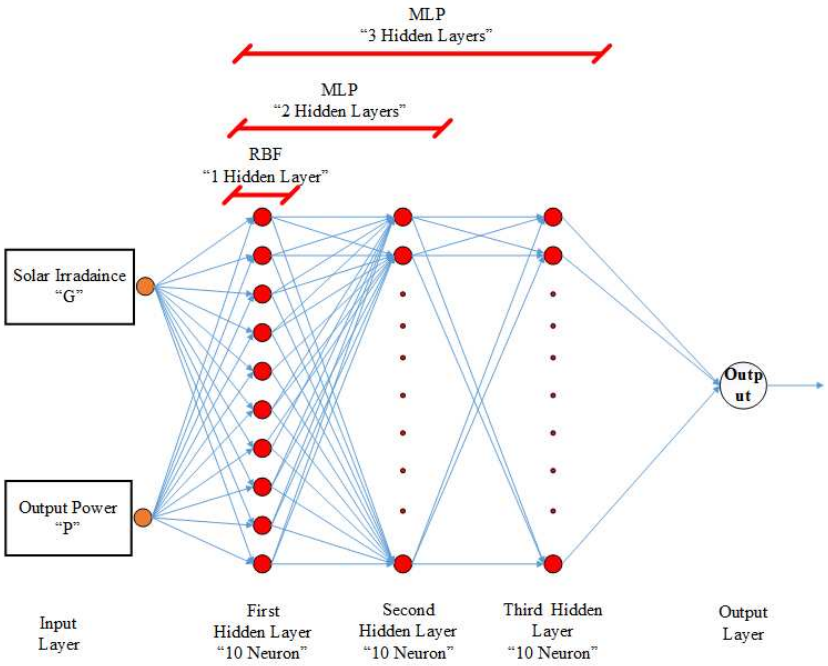

Figure 13. RBF vs. MLP

Moreover, the RBF is more adequate compared with the MLP is due to the digital nature of the failure associated with the PV system; the individual PV modules are completely "ok" or completely "off", where no "intermediate" failure occurs.

The selection of the ANN network was based on the results obtained from testing and comparison of the two networks in terms of the overall detection accuracy and required computational time. Figures 14 (a) and (b), show the overall detection accuracy of two MLP networks with 2 and 3 hidden layers, respectively. There is only a small difference in the accuracy (+0.2%) whereas the computational time increased by 155ms, refer to Figure 14 (c).

When comparing an RBF with an MLP network consisting of 3 hidden layers the detection accuracy increased by a small margin (+0.5%) whilst the corresponding computational time

increased considerably from 45ms to 290ms. Consequently, increasing the time of which a PV fault can be detected as well as the overall energy consumption of the microcontroller power unit.

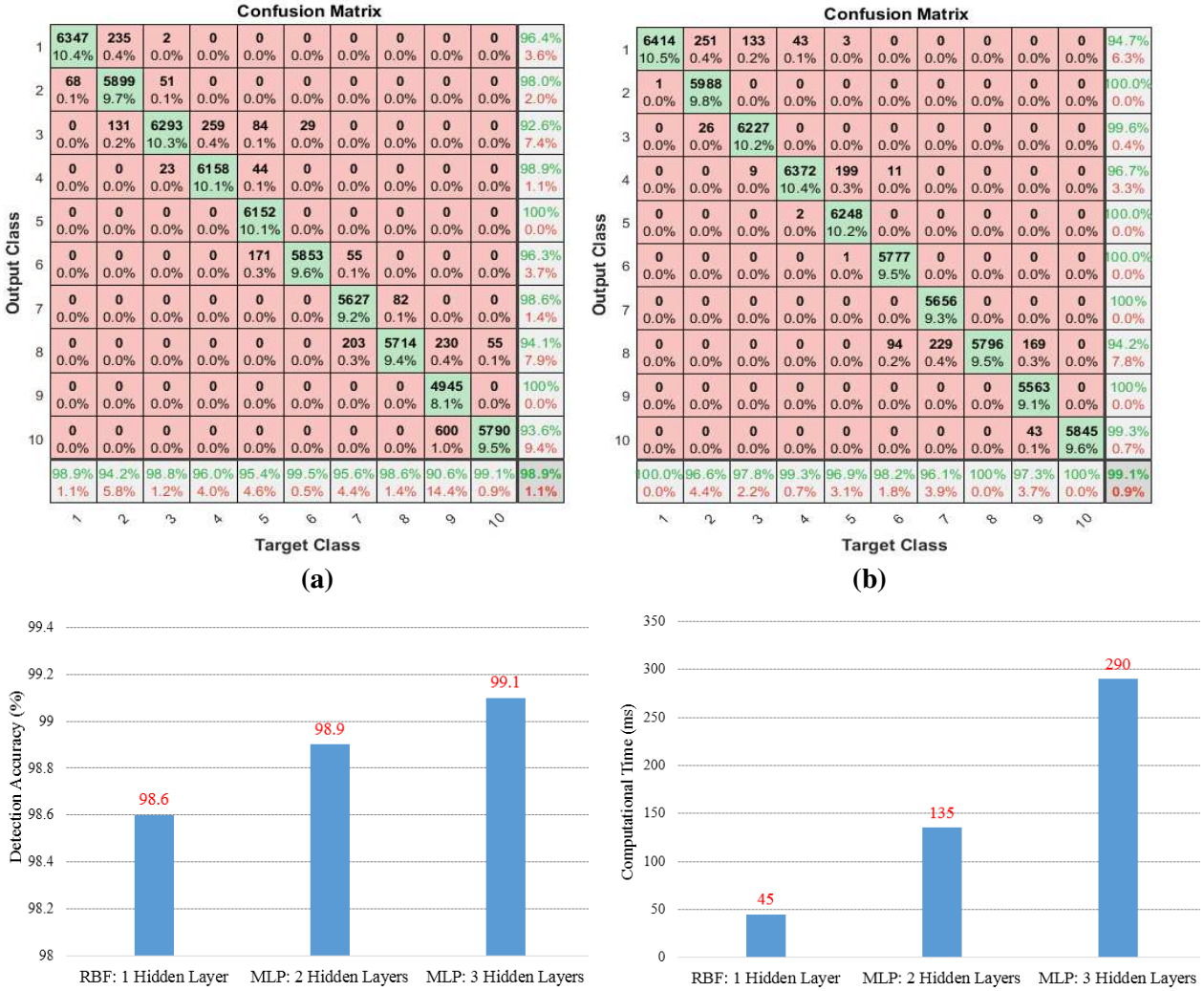

Figure 14. Output detecting accuracy of the MLP networks vs. RBF network. (a) 2 hidden layers, (b) 3 hidden layers, (c) Detection accuracy and the minimum computational time difference

3.9 t-test statistical analysis

In practice, comparing the competence of ANN models with conventional statistical techniques is critical, as uncomplicated statistical models could result the same detection accuracy compared with complicated ANN models. Therefore, we have used the well-established t-test technique that uses the mean value of two tests (in our case normal operation vs number of faulty PV module) and resulting a t-test value, this test has been verified using Minitab software.

With a confidence of 99%, in theory, if the t-test value is greater than 2.58, therefore, there is a significant difference in the two tested value, therefore a fault is ascertained in the PV system.

During no shading conditions, two tests were performed, including one faulty and nine faulty PV modules in the PV string, results are shown in Figures 15(a) and (b). It is clearly notable that the t-test is beyond the limit of 2.58, therefore a fault is detected in the PV string.

Whistle testing the same faulty conditions under partial shading condition, the result of the t-test does not show a significant difference, as the t-test value is still within the theoretical threshold of 2.58 as can ben seen in Figures 15(c) and (d). This result confirms that even sophisticated statistical technique such as t-test can only be used in some cases to detect the faults in the PV string, while, for example, under shading conditions, it fails to determine the difference between the normal operation and one faulty or nine faulty PV modules.

In conclusion, ANN model is therefore having a benefit over statistical-based techniques, as ANN models can determine the difference of the power and irradiance levels and has the possibility to distinguish the variations of these parameters including shading and non-shading conditions.

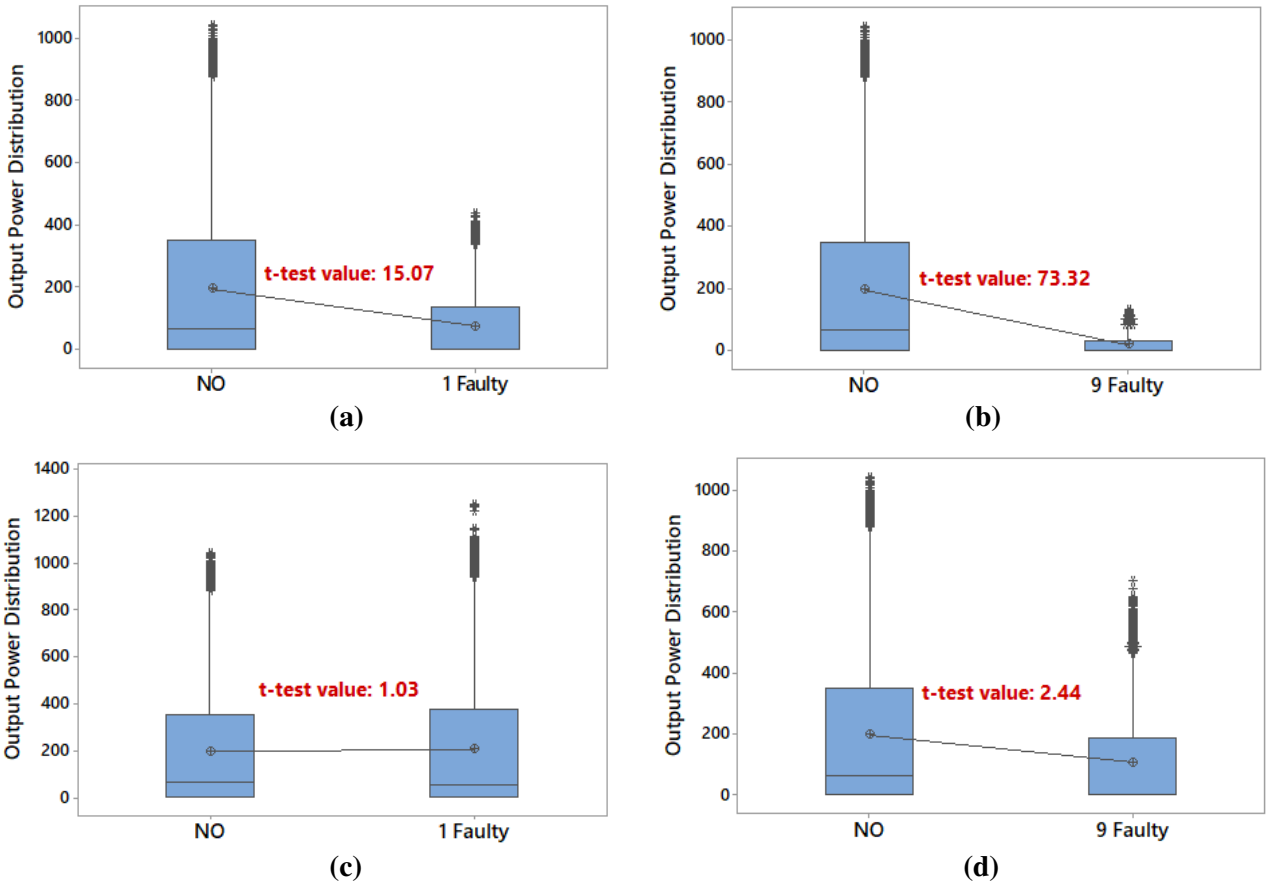

Figure 15. Output t-test value. (a) Normal operation vs one faulty PV module, without partial shading "sunny day", (b) Normal operation vs nine faulty PV modules in the PV string, without partial shading, (c) Normal operation vs one faulty PV module, data captured under partial shading scenario, (d) Normal operation vs nine faulty PV modules in the PV string, without partial shading

4. Results

This section reports on the accuracy of the ANN through the implementation of the selected methodology (M4) from section 3.6, as this methodology had achieved the highest fault detection accuracy. Furthermore, the developed ANN using M4 is trained with a 'scaled-up' PV system and reduced data set, refer to section 4.3. Note that the data presented in this section for testing the actual accuracy of the ANN has not been previously used for training the ANN network, previously discussed in section 3, reiterating the authenticity and integrity of our ANN.

4.1. Partial shading results

The developed fault detection algorithm was subject to various experiments, in order to validate its resilience, robustness and accuracy. The sample-set was collected over two weeks with the first week testing under partial shading conditions and the latter under overcast conditions. Each scenario persists for an entire day with a different fault applied to the examined PV system illustrated previously in Figure 2.

The first week was based on validating the accuracy of the network based on the data collected on partial shading. The solar irradiance for week-one is represented in Figure 16.

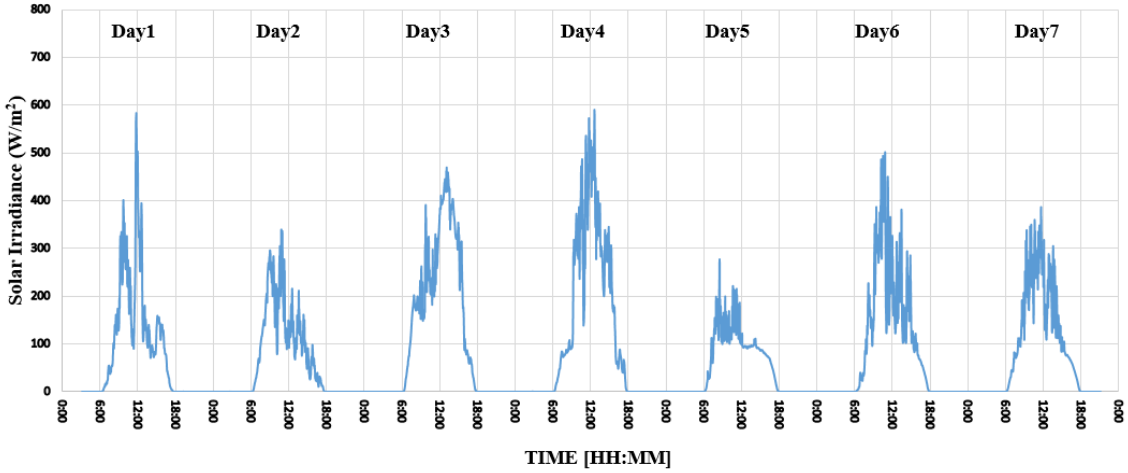

Figure 16. Solar irradiance of PV system for week one under partial shading conditions

The total output power of the system in question under different test conditions is represented in Figure 17. The system is operating without any applied faults on the first day; hence, the total output power is at its peak. During the duration of the week, as various faults are applied on a day to day basis, the total output power decays. With the system generating its lowest output power on day 6 with 7 faults applied. Note day-five has a low output power even though the system is running without any applied faults, and this is due to the corresponding solar irradiance being at its lowest for that day, represented in Figure 16.

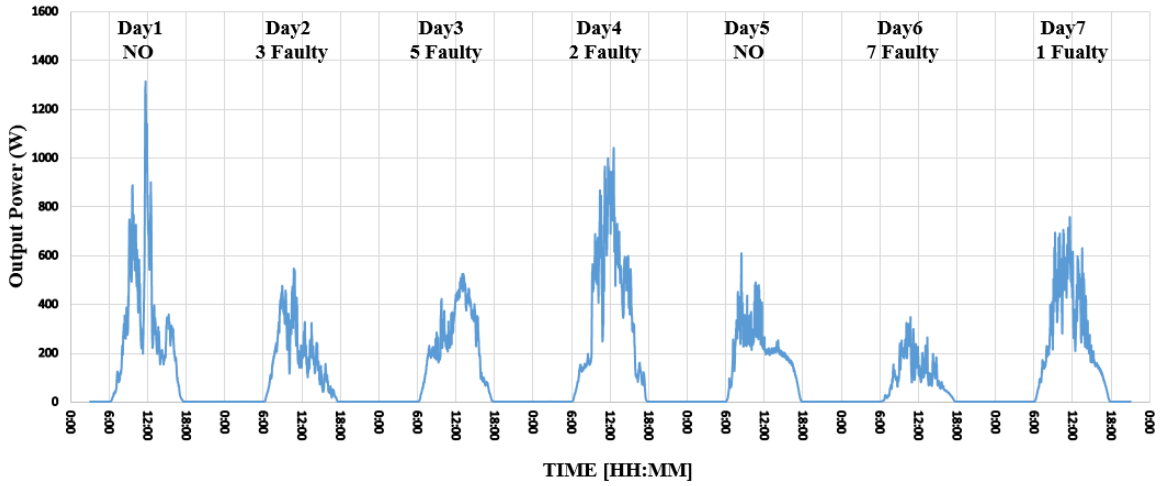

Figure 17. Total output power of PV system for week one under partial shading conditions

The authentication of the accuracy of the developed ANN under partial shading conditions over the week is represented by the output classification matrices, shown in Figure 18. The green and red cells of the matrix represent the number of correct and incorrect classifications by the ANN, respectively. The grey cells represent the total detection accuracy with respect to each row and column.

The overall accuracy of the system under partial shading conditions was 97.9%, as shown in Figure 18. Out of 1413 samples, there are 1373 samples for NO (normal operation) correctly classified, whereas 40 samples are misclassified as F2, F3 or F4, this corresponds to 2.8% faulty classifications during NO and shading conditions. On the other hand, 666 samples are correctly classified as F2, while some samples are misclassified as either F1 or F3, this is due to the change of the solar irradiance affecting the PV system during the fourth examined day.

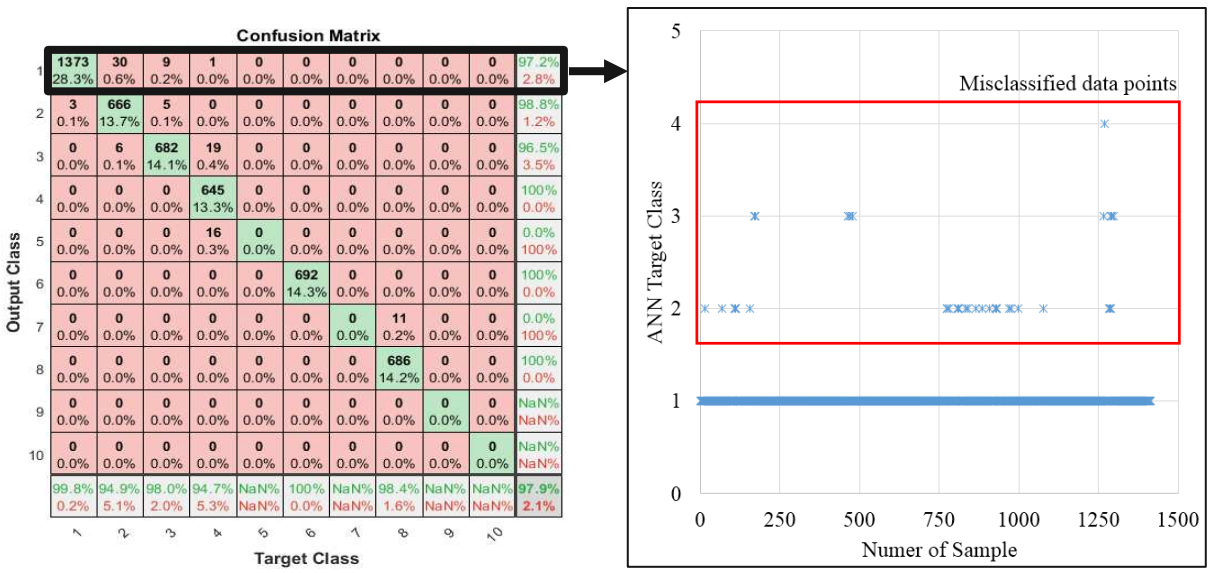

Figure 18. Confusion Matrix for ANN under partial shading conditions

4.2. Overcast Results

The second week was based on validating the accuracy of the network with regards to the data collected for overcast conditions (partially cloudy and overcast). The solar irradiance for week one is shown in Figure 19.

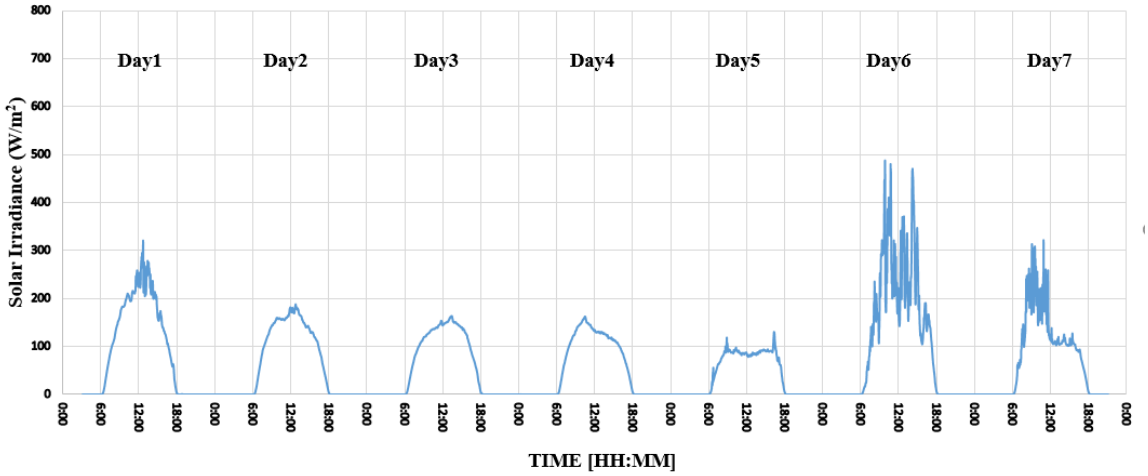

Figure 19. Solar irradiance of PV system for week two under overcast conditions

The total output power of the system in question under different test conditions is represented in Figure 20. The system is operating without any applied faults (normal operation) on the first day, but the total output power is not at its peak, whereas for the sixth day 1-fault is applied but it has the highest total output power for the week, this is due to the solar irradiance being significantly higher on day-six as compared to any other day of the week, including day-one.

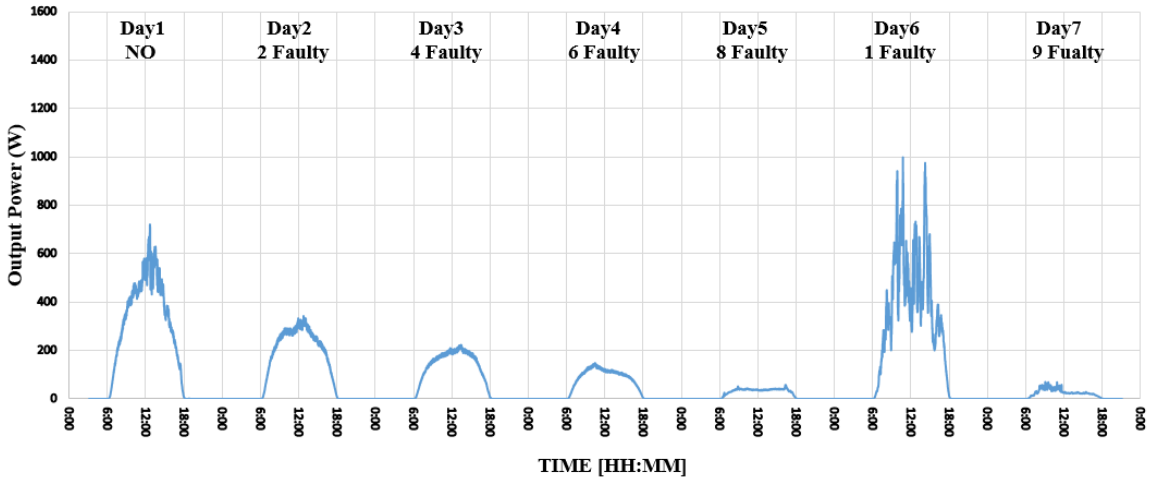

Figure 20. Total output power of PV system for week two under overcast conditions

As shown in Figure 21, the overall accuracy of the system for overcast conditions was 96.5%. Total of 710 samples for normal operation "NO" are correctly classified. This corresponds to 14.2% of all tested samples. Similarly, 661 samples are correctly classified as F2, corresponding to 13.2% of all samples. In row 1, 34 samples of NO are incorrectly classified as F1 corresponding to 0.7%. This was because the output power during normal operation mode and 1-faulty PV module are similar, particularly during partial shading conditions.

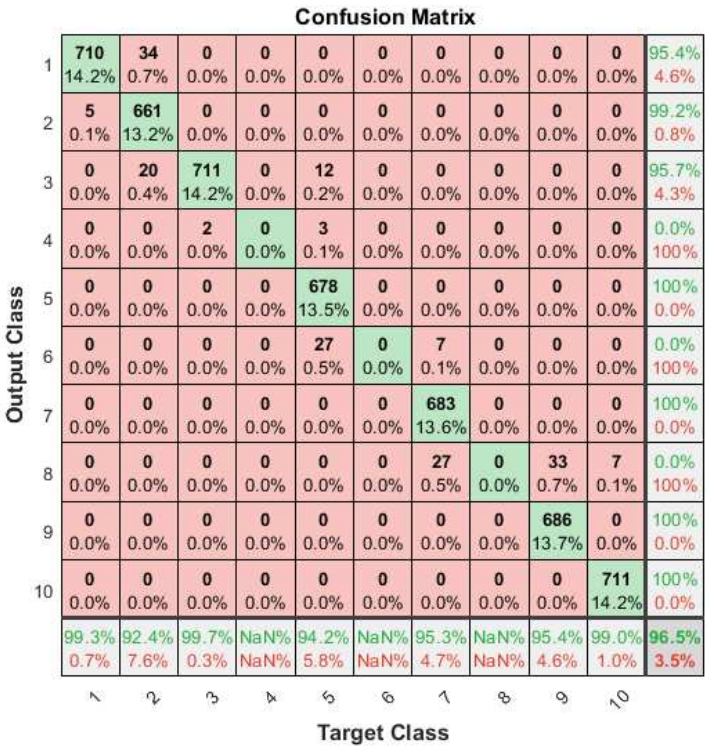

Figure 21. Confusion Matrix for ANN under overcast conditions

The ANN network performed to a higher accuracy in partial shading conditions as compared to overcast conditions. However, the overall accuracy of both systems was over 95% with a difference of 1.4% in terms of accuracy, between the two networks. The overcast conditions did not have a significant impact on the accuracy of the ANN, demonstrating the robustness of the system. It is important to note that although the sample data from both conditions was the same, the actual content of the data varied (the solar irradiance was much lower for overcast conditions as compared to partial shading). The developed ANN was able to handle this variance in the input data, through its training and validation, testifying its effectiveness through the overall detection accuracy for both conditions, as shown in the respective confusion matrices, Figures 18 and 21.

4.3. ANN results with different PV system

To validate the detection accuracy of the developed ANN, the network was tested with a different PV plant (refer to Figure 22). The plant contained four PV strings, each consisting of 8 PV panels with all strings connected in series. The switches on the inverter allowed the switching on-off of a whole string. However, only one string was to be switched off at any given time representing 8 faults. If two strings were taken off-line, the occurred faults would equal 16, this was not within the scope of this research. The total capacity of the examined PV system is equal to 4.16 kW.

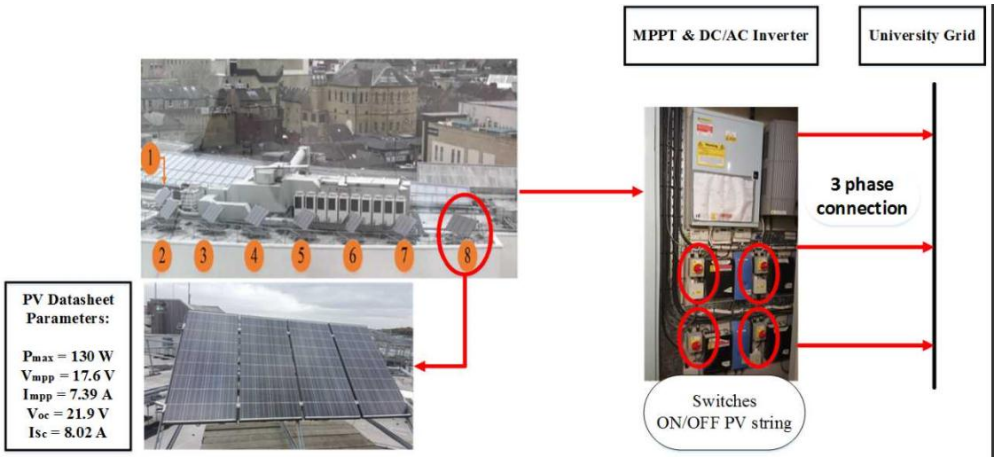

(a)

(b)

Figure 22. **(a)** Actual setup of PV system, **(b)** PV system schematic for test case study

The test procedure involved inducing 8-faults by switching off a complete string, followed by normal operation for the next day, refer to Table 3. The solar irradiance and total power for the duration of the testing period is represented in Figure 23; comprising of overcast and partial shading conditions.

Table 3. Methodology for test case

No. Days	Condition Applied
1	NO
2	1st string is disconnected
3	NO
4	2nd string is disconnected
5	NO
6	3rd string is disconnected
7	NO
8	4th string is disconnected

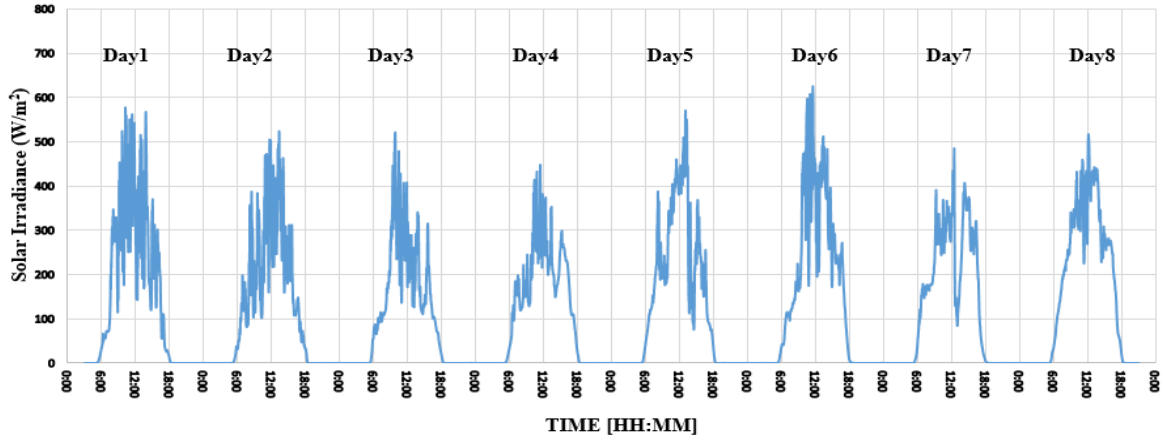

(a)

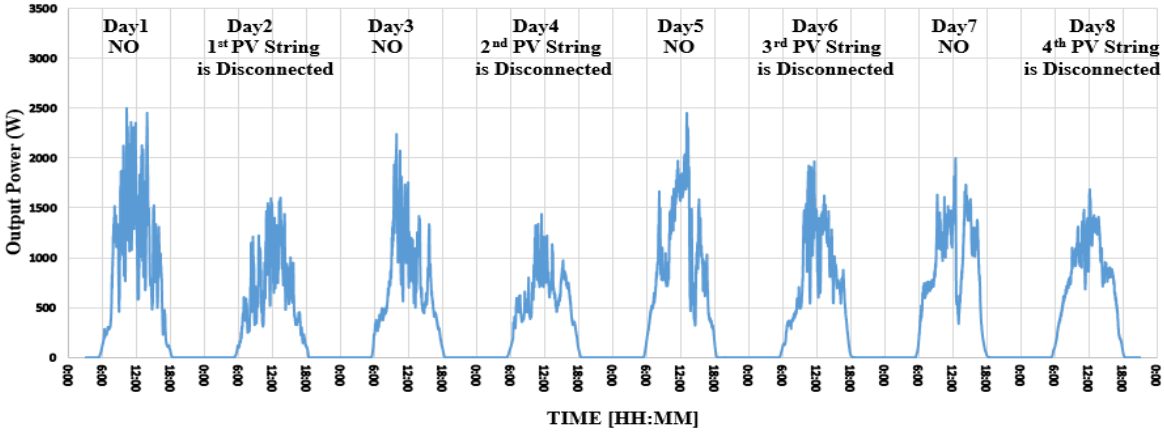

(b)

Figure 23. **(a)** Solar irradiance, **(b)** Output power for test case

Figure 24 illustrates the overall detection accuracy of the developed ANN for the test case PV system shown in Figure 22. Before extracting any conclusions on the accuracy of the ANN, based on the comparison of the two PV systems, key factors need to be considered. The first important factor is the significant variation in the total power capacity of the two systems (2.2 kW and 4.16 kW). Achieving an accuracy of over 96% for both PV systems, the ANN has shown it is highly adaptable to various capacity of PV systems. Another critical factor was the substantial difference of the sample data for training the ANN. The first PV system provided the ANN with 'rich' training data consisting of every hour of the day, for a duration of 10-weeks. Whereas, the latter system reported in this sub-section decreased the amount of training data to 8-days. Nevertheless, the overall detection accuracy of the ANN for both PV systems boasted results of over 96%. This again testifies to the reliability, adaptability and successful implementation of our proposed ANN.

In order to validate the latter ANN network, an evaluation of the total detection accuracy was carried out every two days interval. The reason for the selection of 'two-day' intervals was due to the first day consisting of normal operation "NO" followed by 8-faulty "F8" (induced faults by switching of a whole string, refer to, Figure 22(b)) for the second day. The ANN network original MATLAB code is shown in Appendix A.

Hence, the results of the ANN network during the first two days including NO "as in first day" and 8-faulty PV modules "as in the second day" is shown in Figure 24(a). The attained detection accuracy is equal to 97.4%. The main factor that the detection accuracy slightly dropped during 8-faulty "F8" mode, was due to 26 samples being incorrectly classified as either 9-faulty or 10-faulty PV modules, resulting in a 2.1% decrease in accuracy.

The following 2-days (days 3-4), shown in Figure 24(b), experienced an increase in the overall detection accuracy of the ANN at 98.0%. The improvement in the overall accuracy was due to the ANN misclassifying 16 samples as 9-faulty or 10-faulty, when the actual fault induced was 8-faulty "F8" relating to an error of 1.3%.

In contrast to the above pattern of gradual increase in the overall detection accuracy as the week progressed, day 5 and 6, shown in Figure 24(c) showed signs of deterioration in the over accuracy of the ANN (96.6%). A total of 43 samples were incorrectly classified as 9-faulty or 10-faulty instead of 8-faulty.

The last two days (days 7 and 8), shown in Figure 24(d) indicated towards an improvement in the overall detection accuracy of the network, with a total accuracy of an impressive 98.1%. Similarly, to the first two days (days 3 and 4), 15 samples were incorrectly classified as either 9-faulty or 10-faulty PV modules, whereas the induced fault consisted of 8-faulty, this led to the reduction in the overall accuracy by about 0.9%.

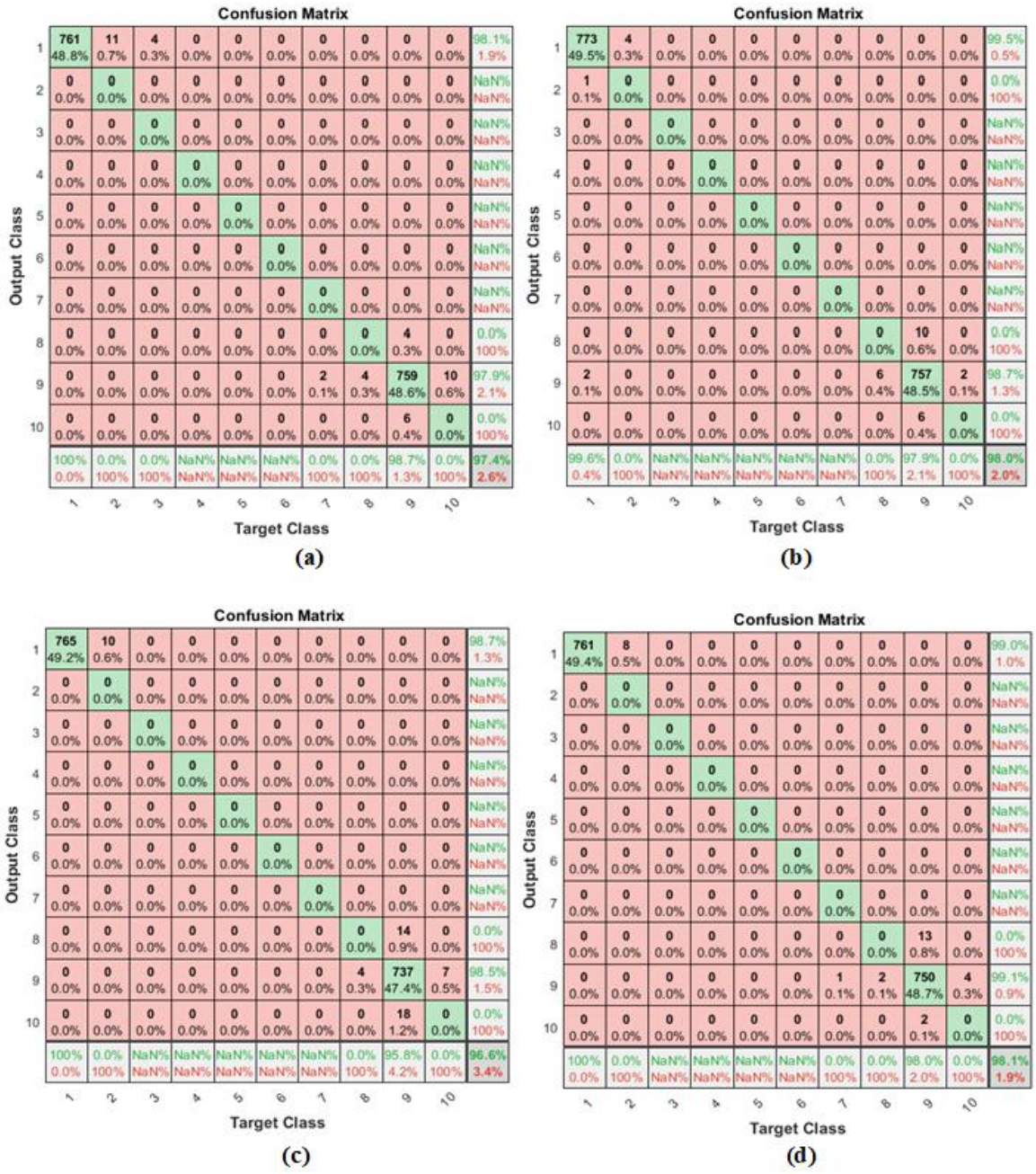

Figure 24. Classification Confusion Matrices for the ANN based on the test case PV system shown previously in Figure 22. **(a)** Accuracy is 97.4% for the first 2 days, **(b)** 98.0% for days 3 and 4, **(c)** 96.6% for days 5 and 6, **(d)** 98.1% for the last 2 days (day 7 and 8)

5. Comparative Study

This section evaluates and compares the new research outcomes [24, and 26-28] in the field of ANN PV fault detection systems against our proposed methodology. A comprehensive evaluation of the methodologies is summarized in Table 4.

As illustrated, all recent ANN-based PV fault detection systems require a large number of input parameters for the ANN network to operate; hence, the algorithm becomes more complex in terms of the practicality as well as the required historical data for the ANN training/validation process.

568 However, in this article, the proposed ANN network only requires two input parameters in order
569 to activate, namely the irradiance and the output power, while there is no need of any other PV
570 parameters such as the V_{mpp} and I_{mpp} as appear in all other recent algorithms [24, and 26-28].

571 The other advantage of our proposed algorithm is that the ambient temperature has not been
572 included in the ANN architecture. Hence, temperature sensors are no longer required in the PV
573 installation, as this is required by the algorithms proposed by [24] and [28].

574 According to our method, the ANN detection accuracy is ranging from 96.5%~98.1% in normal
575 operation (NO) and partial shading conditions, respectively. So far, the obtained PV fault detection
576 accuracy is considered the highest, as illustrated in Table 4.

577 Based on the examined PV installations shown earlier in Figures 2(a) and 22(a), the data
578 acquisition of the produced power occur at the DC side after the MPPT unit is placed. This place
579 of sampling data can generally not be taken for granted to be expandable to other PV systems since
580 not many commercial inverters offer this signal to be extracted. Taking this restraint into
581 consideration, this becomes the main limitation of the proposed model developed in this article.

Table 4. Comparitive study of recent ANN-based PV fault detection algorithms [24, and 26-28] and our proposed method

Ref.	Year	Number of examined PV modules "connected in series"	ANN Methodology – required input parameters								ANN detection accuracy (%)	
			G	T_{amb}	P	I_{sc}	V_{oc}	I_{mpp}	V_{mpp}	No. of required parameters	Normal Operation	Partial Shading
[24]	2016	Four 25% each setp	✓	✓	✓	✗	✗	✓	✓	5	90.3~97	max:90.3
[26]	2017	Up to Five 20% each step	✓	✗	✗	✓	✓	✓	✓	5	96.5	n/a
[27]	2018	Five 20% each step	✗	✗	✓	✓	✓	✓	✓	4	97.1~95.3	87.3~92.1
[28]	2019	Up to four 25% each step	✓	✓	✓	✗	✗	✓	✓	5	87.4~98.5	max: 66.45
Our proposed algorithm	2020	Ten 10% each step	✓	✗	✓	✗	✗	✗	✗	2	98.1%	96.5%

6. Conclusion

In this article, we have presented four different methodologies to detect PV faults based on two inputs parameters; solar irradiance and output power. It was found that the ANN accuracy increased up to 98.1% based on the implementation of the fourth methodology consisting of data normalisation as well as mapping of solar irradiance against output PV power. Hence, this methodology has been tested on two different PV installations, with significantly different electrical parameters.

Results show that the developed ANN network accurately detected PV faults in the range of 96.5-98.1% during normal operational mode, where no shading/overcast is present. Whereas, during partial shading conditions, the minimum ANN network accuracy deteriorated to was 96.2%. This outcome is based on the evaluation of our ANN on two differing PV installations, demonstrating the robustness and adaptability of the proposed network architecture.

In future, it is intended to enhance the accuracy of the developed ANN network through the evaluation of different methodologies comprising of different ANN input parameters as well as using deep learning methods to enhance the capabilities of the ANN neurons during training/validation.

7. References

1. Di Piazza, M. C., Viola, F., & Vitale, G. (2018). Evaluation of ground currents in a PV system with high frequency modeling. International Journal of Renewable Energy Research, 8(3), 1770-1778.
2. Dhimish, M., Holmes, V., Mehrdadi, B., Dales, M., Chong, B., & Zhang, L. (2017). Seven indicators variations for multiple PV array configurations under partial shading and faulty PV conditions. Renewable Energy, 113, 438-460.
3. Mansouri, M., Hajji, M., Trabelsi, M., Harkat, M. F., Al-khazraji, A., Livera, A., ... & Nounou, M. (2018). An effective statistical fault detection technique for grid connected photovoltaic systems based on an improved generalized likelihood ratio test. Energy, 159, 842-856.
4. Dhimish, M., & Holmes, V. (2016). Fault detection algorithm for grid-connected photovoltaic plants. Solar Energy, 137, 236-245.
5. Tadj, M., Benmouiza, K., Cheknane, A., & Silvestre, S. (2014). Improving the performance of PV systems by faults detection using GISTEL approach. Energy conversion and management, 80, 298-304.
6. Mellit, A., & Pavan, A. M. (2010). A 24-h forecast of solar irradiance using artificial neural network: Application for performance prediction of a grid-connected PV plant at Trieste, Italy. Solar Energy, 84(5), 807-821.
7. Takashima, T., Yamaguchi, J., Otani, K., Oozeki, T., Kato, K., & Ishida, M. (2009). Experimental studies of fault location in PV module strings. Solar Energy Materials and Solar Cells, 93(6-7), 1079-1082.
8. Dhimish, M., Mather, P., & Holmes, V. (2018). Evaluating power loss and performance ratio of hot-spotted photovoltaic modules. IEEE Transactions on Electron Devices, 65(12), 5419-5427.
9. L. Schirone, F.P. Califano, M. PastenaFault detection in a photovoltaic plant by time domain reflectometry Prog. Photovolt. Res. App, 2 (1994), pp. 35-44.

10. S. Silvestre, M.A. da Silva, A. Chouder, D. Guasch, E. Karatepe New procedure for fault detection in grid connected PV systems based on the evaluation of current and voltage indicators Energy Convers. Manag., 86 (2014), pp. 241-249.
11. Li, X., Wen, H., Hu, Y., & Jiang, L. (2019). Drift-free current sensorless MPPT algorithm in photovoltaic systems. Solar Energy, 177, 118-126.
12. W. Yuchuan, L. Qinli, S. YaqinApplication of BP neural network fault diagnosis in solar Photovoltaic System Proceedings of the IEEE International Conference on Mechatronics and Automation, Changchun, China (2009), pp. 9-12
13. W.T. Miller III, F.H. Glanz, L.G. Kraft IIICmas: an associative neural network alternative to backpropagation Proc IEEE, 78 (1990), pp. 1561-1567
14. Ashok, V., Yadav, A., & Naik, V. K. (2019). Fault Detection and Classification of Multi-location and Evolving Faults in Double-Circuit Transmission Line Using ANN. In Soft Computing in Data Analytics (pp. 307-317). Springer, Singapore.
15. Pan, T., Chen, J., Zhou, Z., Wang, C., & He, S. (2019). A Novel Deep Learning Network via Multi-Scale Inner Product with Locally Connected Feature Extraction for Intelligent Fault Detection. IEEE Transactions on Industrial Informatics.
16. Belaout, A., Krim, F., Mellit, A., Talbi, B., & Arabi, A. (2018). Multiclass adaptive neuro-fuzzy classifier and feature selection techniques for photovoltaic array fault detection and classification. Renewable energy, 127, 548-558.
17. Belaout, A., Krim, F., Mellit, A., Talbi, B., & Arabi, A. (2018). Multiclass adaptive neuro-fuzzy classifier and feature selection techniques for photovoltaic array fault detection and classification. Renewable energy, 127, 548-558.
18. Malik, H., & Yadav, A. (2018). EMD and ANN based intelligent model for bearing fault diagnosis. Journal of Intelligent & Fuzzy Systems, (Preprint), 1-12.
19. Javed, W., Chen, D., Farrag, M. E., & Xu, Y. (2019). System Configuration, Fault Detection, Location, Isolation and Restoration: A Review on LVDC Microgrid Protections. Energies, 12(6), 1001.
20. A. Lapedes, R. FarberNonlinear signal processing using neural networks (1987)
21. Mellit, A., Sağlam, S., & Kalogirou, S. A. (2013). Artificial neural network-based model for estimating the produced power of a photovoltaic module. Renewable Energy, 60, 71-78.
22. Polo, F. A. O., Bermejo, J. F., Fernández, J. F. G., & Márquez, A. C. (2015). Failure mode prediction and energy forecasting of PV plants to assist dynamic maintenance tasks by ANN based models. Renewable Energy, 81, 227-238.
23. Yagi, Y., Kishi, H., Hagihara, R., Tanaka, T., Kozuma, S., Ishida, T., ... & Kiyama, S. (2003). Diagnostic technology and an expert system for photovoltaic systems using the learning method. Solar energy materials and solar cells, 75(3), 655-663.
24. Chine, W., Mellit, A., Lughi, V., Malek, A., Sulligoi, G., & Pavan, A. M. (2016). A novel fault diagnosis technique for photovoltaic systems based on artificial neural networks. Renewable Energy, 90, 501-512.
25. Yuchuan Wu, Qinli Lan and Yaqin Sun, "Application of BP neural network fault diagnosis in solar photovoltaic system," 2009 International Conference on Mechatronics and Automation, Changchun, 2009, pp. 2581-2585.
26. Karmacharya, I. M., & Gokaraju, R. (2017). Fault location in ungrounded photovoltaic system using wavelets and ANN. IEEE Transactions on Power Delivery, 33(2), 549-559.
27. Dhimish, M., Holmes, V., Mehrdadi, B., & Dales, M. (2018). Comparing Mamdani Sugeno fuzzy logic and RBF ANN network for PV fault detection. Renewable energy, 117, 257-274.
28. Fadhel, S., Delpha, C., Diallo, D., Bahri, I., Migan, A., Trabelsi, M., & Mimouni, M. F. (2019). PV shading fault detection and classification based on IV curve using principal component analysis: Application to isolated PV system. Solar Energy, 179, 1-10.

Appendix A

ANN Matlab Code:

```
function [y1] = myNeuralNetworkFunction(x1)

% Input 1
x1_step1.xoffset = [0;0];
x1_step1.gain = [2;2];
x1_step1.ymin = -1;

% Layer 1
b1 = [-0.53379789162008717263;-5.6867963876778855337;10.17789601263983456;-2.5991370178094546084;-
0.95996065238647498852;2.9461760878212293058;4.3468884838846104657;-1.6827716763193365512;-
15.784457032110500663;18.01460876010765233];

IW1_1 = [10.739580122585271837 -11.159248213784534798;2.5403215144122435198 -
0.56388784665404756424;-15.530906692487940646 25.724533995852432611;2.6108726483375148675
2.8644466106623927004;2.3492627965250321154 -3.9135393841679908533;2.5621241841492614633
1.3108436436418966498;-18.156042599742011845 22.592529645218835554;-2.2026222558534906959
4.5796412164194322258;10.73037657323408034 -26.46367903771555774;-4.6700671639881869979
22.673036080767015932];

% Layer 2

b2 = [-0.60795246307066741487;0.52920177750850172504;0.87317087958293260197;-
0.77428730832701464504;0.80856340475453847283;-0.98776905950334870088;-
0.038084773428153848029;0.17631768142364898089;0.1177441519341838605;-1.2286308806154839779];

LW2_1 = [-16.218127732052877832 -0.61842039136869231264 13.65432479360931417
0.0279526869588864052 -1.5457829250363672724 -4.5249730228320954595 29.031811827208226617
1.3545922631578695139 -7.4451922992102366194 2.1032270854732173504;-1.8610677877454995244 -
0.13584261850222981161 14.599061786278145547 0.98142879231714974519 0.023068305715024127467
1.2729092739892586827 17.352259289313366253 -1.7969598569705769187 -7.5890283129856896949
5.3777628244524660062;0.0176905085802088919 7 -1.7872590063111608583 14.453052562066568854 -
0.28584189135600646114 -2.2943096899107273678 4.6075393554886687753 2.5732414558365808155 -
1.3164653264959451651 -9.2113122319186704345 3.9165651867640507433;0.78870635459690852098
0.45655538810872159372 15.726589320682379025 1.2188914303559659214 1.5572518953867149349 -
0.74512350082267531093 -12.537359667453197076 0.55369386754372895698 -8.5220919780286497058
3.4338668969512400331;2.0317783279326593338 -1.1142040895525726629 0.31670104901807094588
0.97848656798353517715 0.76022477810981570201 3.7280444386583488914 -9.8244365967376374726
0.52810244259625593877 -11.604561582830564603 3.3371779646911083894;1.7526128243198901835
0.18517512931874907656 -15.506889259234823086 0.96516150852280624406 0.37972493906172594125 -
1.1950923243193563028 -5.2382773533629025664 0.77967472280614491531 -11.860434415464807145
5.1071998684124046974;2.1381733507637172842 0.056596023834588657375 -13.298494169561720923
0.11021173484657678654 1.2536020059998913556 1.7661104686248074724 -5.336103540167647985
0.23036465741826600562 3.3863911471888354932 8.9226575295582417624;3.6723972390395536181
0.87284720834851448057 -8.4578343073060278101 -0.044134247790334736605 0.37388197719519100648 -
1.0196077545498973826 -5.8551819327672580684 -0.11479275509819439338 17.324612120669645066
6.7927117492973421164;6.6441975543224023326 0.44978145240560007956 -8.0408855433529229373 -
0.81189573510752477414 0.7060671169563150773 1.493396637034419383 -5.7368690002926161497 -
0.87186633673562252689 16.908781753661273228 -9.5834534191820850424;3.0982763799864270204
0.49939749005411848692 -8.9893465264005989468 0.36043960291007642871 0.22646282549337756751 -
4.3925487668578648837 -5.6103623569920149095 0.51747719198805008922 18.039904522133820564 -
27.296588790470323715];
```

```
% ===== SIMULATION ========
Q = size(x1,1); % samples

x1 = x1'; % Input 1
xp1 = mapminmax_apply(x1,x1_step1);

a1 = tansig_apply(repmat(b1,1,Q) + IW1_1*xp1); % Layer 1

a2 = softmax_apply(repmat(b2,1,Q) + LW2_1*a1); % Layer 2

y1 = a2; % Output 1
y1 = y1';
end

function y = mapminmax_apply(x,settings) % Map Minimum and Maximum Input Processing Function
y = bsxfun(@minus,x,settings.xoffset);
y = bsxfun(@times,y,settings.gain);
y = bsxfun(@plus,y,settings.ymin);
end

function a = softmax_apply(n,~) % Competitive Soft Transfer Function
if isa(n,'gpuArray')
    a = iSoftmaxApplyGPU(n);
else
    a = iSoftmaxApplyCPU(n);
end
end

function a = iSoftmaxApplyCPU(n)
nmax = max(n,[],1);
n = bsxfun(@minus,n,nmax);
numerator = exp(n);
denominator = sum(numerator,1);
denominator(denominator == 0) = 1;
a = bsxfun(@rdivide,numerator,denominator);
end

function a = iSoftmaxApplyGPU(n)
nmax = max(n,[],1);
numerator = arrayfun(@iSoftmaxApplyGPUHelper1,n,nmax);
denominator = sum(numerator,1);
a = arrayfun(@iSoftmaxApplyGPUHelper2,numerator,denominator);
end
function numerator = iSoftmaxApplyGPUHelper1(n,nmax)
numerator = exp(n - nmax);
end
function a = iSoftmaxApplyGPUHelper2(numerator,denominator)
if (denominator == 0)
    a = numerator;
else
    a = numerator ./ denominator;
end
end
function a = tansig_apply(n,~) % Sigmoid Symmetric Transfer Function
a = 2 ./ (1 + exp(-2*n)) - 1;
end
```